# Pattern Formation in Spatially Extended Systems: Interplay of Variability and Noise

Vom Fachbereich Physik
der Technischen Universität Darmstadt
zum Erlangen des Grades
eines Doktors der Naturwissenschaften
(Dr. rer. nat.)

genehmigte

## Dissertation

von

**Dipl.-Phys. Erik Glatt**
aus Mannheim

Darmstadt 2008
D17

| | |
|---|---|
| Referent: | Prof. Dr. Friedemann Kaiser |
| Korreferentin: | Prof. Dr. Barbara Drossel |
| Tag der Einreichung: | 14.05.2008 |
| Tag der Prüfung: | 16.06.2008 |

# Contents

# 1 Introduction

Many spatially extended systems, from physics to biology, show a complex long-range dynamics. In those systems one can observe coherent pattern formation, which is generated by the interplay of the nonlinear components of the system [1, 2, 3]. For a fundamental understanding of the system one has to know the pattern forming mechanisms [4, 5, 6]. However the spatiotemporal dynamics of biological systems is even more complicated, because the omnipresent stochasticity of the systems may play an important role for pattern formation.

Biological systems, in particular on small scales (molecular and microscopic systems), are exposed to large fluctuations and have to be adapted to noise. Hence, if one tries to describe biological systems with low dimensional sets of model equations, one has to include the noise. In the last years it was shown theoretically that noise may play a constructive role in many systems. Examples are: spatiotemporal stochastic resonance [7, 8], coherence resonance [9], noise-induced transitions [10, 11] and noise-based switches for gene expression [12]. A good overview of noise in spatially extended systems is given by J. García-Ojalvo et al. [13] and F. Sagués et al. [14].

There are experimental results, which confirm that biological systems may use noise in a constructive way. Noise may improve the response signal of a neuron [15] and it may help the paddlefish to catch its pray [16]. Furthermore noise does sustain waves in slices of hippocampal astrocytes [3]. In particular the last result supports the assumption that the fluctuations may be important for pattern formation in spatially extended biological systems.

A second omnipresent source of stochasticity in biological systems is the variability. Variability (diversity, heterogeneity) denotes static stochastic differences between otherwise equal elements of a system. It means that e.g. in a colony of bacteria the single cells are slightly different from each other. Lately the existence of variability in populations of bacteria has been confirmed experimentally [17].

Theoretically it was shown that variability can effect the spatiotemporal dynamics of many systems. The influence of parameter variability on the synchronisation of coupled oscillators was investigated by Winfree [18] and Kuramoto [19]. Beyond that it was shown that variability can lead to a more regular dynamics in spatiotemporal chaotic systems [20, 21]. Furthermore variability can play an important role for pattern formation in chains of biochemical oscillators [22]. Recently it was demonstrated, that diversity can cause resonance-like phenomena in networks of nonlinear elements [23, 24].

All the phenomena mentioned above motivate to perform a detailed numerical and analytical study of the interplay of variability and noise in spatially extended systems. This interplay might have a significant influence on pattern formation and synchronisation. In this thesis such a general study of variability and its interplay with noise in some biologically motivated mathematical model systems is performed. The model systems are spatially extended oscillatory and excitable nets. Both, oscillatory and excitable spatiotemporal dynamics, are found in many biological systems, which exhibit pattern formation.

## 1.1 Outline of this Thesis

In the first part of this thesis the model systems and the basic theoretical concepts are presented. In Chapter 2 the Hodgkin-Huxley model, a standard model to describe neuronal dynamics, is introduced. Based on the Hodgkin-Huxley equations a minimal model of neuronal dynamics, the FitzHugh-Nagumo model, is established. Beyond this the temporal and spatiotemporal dynamics of the model equations are discussed in detail. In the last section of this chapter analysis tools to examine the dynamics of spatially extended systems are introduced. Chapter 3 deals with the theoretical basis of variability and noise. The stochastic terms are included in the model equations and their properties are specified. The difference between additive and multiplicative stochastic terms is explained. Furthermore methods to theoretically predict the influence of multiplicative noise and multiplicative variability on the model systems are presented.

The second part of this thesis presents many results from the model equations under the influence of variability and/or noise. In Chapter 4 oscillatory nets of FitzHugh-Nagumo elements are considered, where in the first section of this chapter the interplay of additive variability and additive noise is studied. The second section deals with the interplay of multiplicative variability and multiplicative noise in such nets. Throughout Chapter 5 subexcitable nets of FitzHugh-Nagumo elements are explored. In the first section the interplay of additive variability and additive noise is studied, whereas in the second section of this chapter the multiplicative stochastic terms are examined. Finally, in Section 5.3, the interplay of additive variability and multiplicative variability is studied. Nets of Hodgkin-Huxley elements are considered in Chapter 6, where in the first section oscillatory nets under the influence of variability and noise are examined. The second section discusses the influence of additive variability on excitable nets. In difference to the previous chapters, where only white variability was studied, the variability is considered to be exponentially correlated in Chapter 7. Thereby diffusively coupled nets of FitzHugh-Nagumo elements with additive and multiplicative variability, but without noise, are investigated. In Chapter 8 variability in the coupling strength is introduced and the influence of such a variability on diffusively coupled oscillatory nets of FitzHugh-Nagumo elements is examined.

Finally, Chapter 9 summarises the basic results presented in this thesis and gives possible perspectives for future research.

# 2 Model Systems

One essential characteristics of most neurons is their excitability [25, 26]. Resting in a steady state a small external stimulus can initiate a large amplitude-spike of the membrane potential of such a neuron. After the amplitude spike, which is called action potential, the neuron needs some time to restore its rest state and for this refractory time it is hardly possible to excite the neuron again. The neuron is in the refractory state.

Excitability is not limited to neurons and can be found in a large variety of dynamical systems. One example from biology is the single cell organism Dictyostelium discoideum (slime mould amoebae) [27]. During the aggregation period, which sets in when Dictyostelium is starving, the individual amoebae acts as an excitable systems, where a single cell can be stimulated by the signal molecule cAMP. During its excitation the cell releases the signal molecule which may excite adjacent cells in a colony of Dictyostelium. The cells use this mechanism to communicate and it allows them to form a multicellular assembly. A spatially extended excitable system is called exitable medium.

A second example for a spatially extended excitable system is a forest. A single element in this medium is a tree, where an excitation of the element means that it starts to burn. Such an excitation might occur because of a lightning. Starting from the excited element the adjacent trees may start to burn and a wild fire, which forms a propagating wave front, spreads through the forest. Such waves in exitable media are called excitation waves. They have the particular feature to die out when two of them meet. The reason for this property is the refractory time of the system. For the forest this means that no fire can return until the trees are regrown (forest-fire model [28, 29]). Excitation waves are typical for excitable media and they can be found for instance in colonies of Dictyostelium [1] or in excitable chemical reactions like the Belousov-Zhabotinsky reaction [2, 30].

In this chapter the Hodgkin-Huxley model [31], a standard model to describe excitable neuronal dynamics, is introduced. Based on the Hodgkin-Huxley equations a minimal model to describe excitable dynamics, the FitzHugh-Nagumo model, is established [32, 33, 34]. Beyond this the temporal and spatiotemporal dynamics of the model equations are discussed in detail. They do not only show excitable dynamics, but also oscillatory and bistable behaviour.

To examine the dynamics of the spatially extended model systems a couple of analysis tools are used in this thesis [35, 8, 10]. In the last section of this chapter these tools are shortly introduced.

## 2.1 Hodgkin-Huxley Model

The Hodgkin-Huxley (HH) model, which was established already in 1952, is based on measurements of the flow of electric currents through the surface membrane of squid giant axons [31]. The current can be carried through the membrane either by charging the membrane capacity $C$ or by the flow of ions through voltage-gated ion channels (Fig. 2.1). The ion current is divided into components carried by sodium ions $I_{Na}$, potassium ions $I_K$

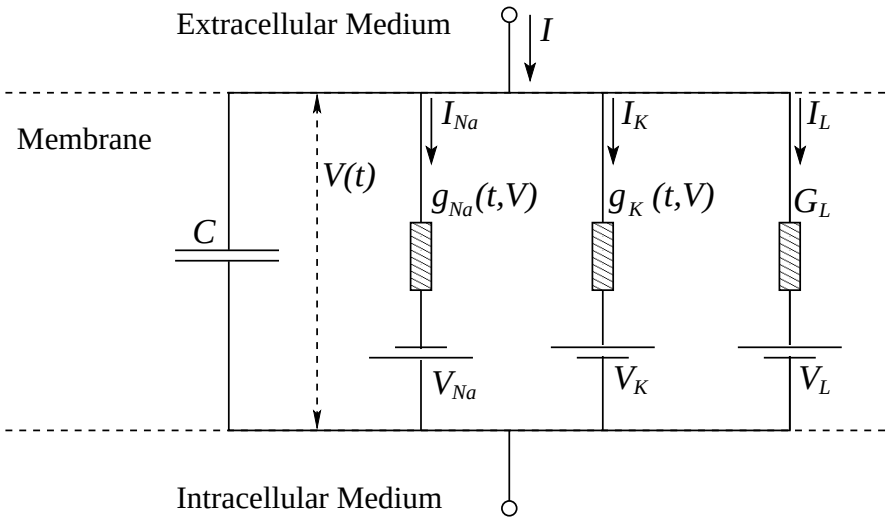


Figure 2.1. Electric circuit representing the membrane of an axon. $V$ is the membrane potential, $C$ is the membrane capacity, $I$ is an external current, $I_{Na}$, $I_K$ and $I_L$ are ion currents and $g_K(V,t)$, $g_{Na}(V,t)$ and $G_L$ are the electrical conductances of the ion channels.

and a small leakage current $I_L$ (chloride and other ions). Furthermore an external current $I$ is assumed. The temporal change of the membrane potential $V$, the voltage inside minus the voltage outside the axon, can thus be described by the following differential equation:

$$C\dot{V} = I - I_K - I_{Na} - I_L. \tag{2.1}$$

The ion currents are given by

$$\begin{aligned} I_K &= g_K(t)(V - V_K) \\ I_{Na} &= g_{Na}(t)(V - V_{Na}) \\ I_L &= G_L(V - V_L), \end{aligned} \tag{2.2}$$

where $V_K$, $V_{Na}$ and $V_L$ are the equilibrium potentials and $g_K(t)$, $g_{Na}(t)$ and $G_L$ the electrical conductances of the ion channels. It is essential for the generation of action potentials that the ion channels are voltage gated and thus time dependent. To describe the dynamics of the ion channels statistically three gating variables $n(t)$, $m(t)$ and $h(t)$ are introduced in the model. These additional variables characterise the probability that an ion channel is open. The opening and closing of the potassium ion channels is given by $n(t)$, while the sodium channels are governed by $m(t)$ and $h(t)$. Using the maximal conductances $G_{Na}$ and $G_K$ and the gating variables one obtains

$$\begin{aligned} g_K(t) &= G_K n(t)^4 \\ g_{Na}(t) &= G_{Na} m(t)^3 h(t). \end{aligned} \tag{2.3}$$

With the Eqs. (2.1), (2.2) and (2.3) one gets the four variable Hodgkin-Huxley model

$$\begin{aligned} \dot{V} &= [I - G_{Na} m^3 h(V - V_{Na}) - G_K n^4 (V - V_K) - G_L(V - V_L)]/C \\ \dot{n} &= \alpha_n(V)(1 - n) - \beta_n(V) n \\ \dot{m} &= \alpha_m(V)(1 - m) - \beta_m(V) m \\ \dot{h} &= \alpha_h(V)(1 - h) - \beta_h(V) h, \end{aligned} \tag{2.4}$$

where $\alpha_i(V)$ and $\beta_i(V)$, with $i \in (n, m, h)$, are exponential functions, which are fitted to the experimental results:

$$\begin{aligned}
\alpha_n(V) &= [0.01(V+55)]/\{1-\exp[-(V+55)/10]\} \\
\beta_n(V) &= p\exp[-(V+65)/80] \\
\alpha_m(V) &= [0.1(V+40)]/\{1-\exp[-(V+40)/10]\} \\
\beta_m(V) &= 4\exp[-(V+65)/18] \\
\alpha_h(V) &= 0.07\exp[-(V+65)/20] \\
\beta_h(V) &= 1/\{1+\exp[-(V+35)/10]\}.
\end{aligned} \tag{2.5}$$

Throughout this thesis the values of the constants

$$\begin{aligned}
&G_{Na} = 120\frac{mmho}{cm^2},\ G_K = 36\frac{mmho}{cm^2},\ G_L = 0.3\frac{mmho}{cm^2}, \\
&V_{Na} = 50mV,\ V_K = -77mV,\ V_L = -54.4mV, \\
&C = 1\frac{\mu F}{cm^2},
\end{aligned} \tag{2.6}$$

which are found for 6.3℃, are used, whereas the parameters $I$ and $p$ are varied [first and second equation of Eqs. (2.4)]. In the original work of Hogkin and Huxley the fit parameter $p$ was set to 0.125. However in this thesis it is shown that noise and variability in this parameter may have a strong influence on the system dynamics.

The Hodgkin-Huxley model can be simplified. This process leads to a set of two differential equations, which is called the reduced Hodgkin-Huxley model [36]. One uses that $m(t)$ evolves much faster than $n(t)$ and $h(t)$ and eliminates the time evolution of this gating variable adiabatically. Furthermore one numerically finds a relation between the gating variables $n(t)$ and $h(t)$, which reads:

$$n(t) + h(t) \approx 0.8. \tag{2.7}$$

With these simplifications one obtains the following equations for the reduced Hodgkin-Huxley model:

$$\begin{aligned}
\dot{V} &= [I - G_{Na}m(V)^3(0.8-n)(V-V_{Na}) - G_K n^4(V-V_K) \\
&\qquad - G_L(V-V_L)]/C \\
\dot{n} &= \alpha_n(V)(1-n) - \beta_n(V)n,
\end{aligned} \tag{2.8}$$

where

$$m(V) = \alpha_m(V)/[\alpha_m(V) + \beta_m(V)]. \tag{2.9}$$

These equations can be handled much easier analytically and numerically than the full model equations [Eqs. (2.4)]. Furthermore it allows an intuitive understanding of the mathematics of action potential generation and hence of excitable dynamics in general. This will be shown in the next subsection.

### 2.1.1 Temporal Dynamics of the Hodgkin-Huxley Model

To determine the temporal dynamics of the Hodgkin-Huxley model [Eqs. (2.4)] a stability analysis in dependency on the model parameters $p$ and $I$ is performed. The result is displayed in Fig. 2.2(a). One can distinguish three different dynamical regimes:

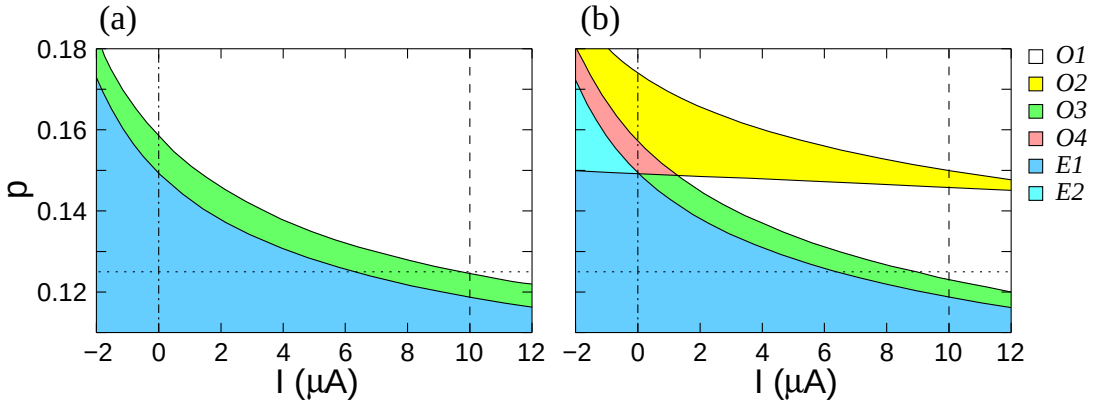


Figure 2.2. Stability analysis of the Hodgkin-Huxley model in dependency on the parameters $I$ and $p$. (a): For the full model [Eqs. (2.4)]. (b): For the reduced model [Eqs. (2.8)]. (—) boundaries of the dynamical regimes, (- · -) $I = 0\mu A$, (- -) $I = 10\mu A$, (· ·) $p = 0.125$. An explanation of the different dynamical regimes is given in the text.

- The excitable regime $E1$: The only attractor is a stable focus. After a transient and without a perturbation the system will rest in this fixed point for all times [Fig. 2.3(a)].

- The oscillatory regime $O1$: One finds a stable limit cycle around an unstable focus and the system exhibits oscillatory dynamics [Fig. 2.3(c)].

- The regime $O3$: A stable focus and a stable limit cycle, separated by an unstable limit cycle, coexist. The system can either rest in the fixed point or it can show oscillatory dynamics.

The stability analysis of the reduced Hodgkin-Huxley model [Eqs. (2.8)] is displayed in Fig. 2.2(b). It reveals additionally three dynamical regimes:

- The excitable regime $E2$: This regime has one stable focus and it shows the same dynamics as the regime $E1$, but it has additionally one unstable focus and one saddle point.

- The oscillatory regime $O2$: This regime, which shows oscillatory dynamics, has one unstable focus and a stable limit cycle as the regime $O1$, but it has additionally one unstable focus and one saddle point.

- The regime $O4$: One again has, as for $O3$, the coexistence of two attractors, one focus and one limit cycle, but this regime has additionally one unstable focus and one saddle point.

The temporal dynamics of the HH model in regime $E1$ is of great interest, even though, without a perturbation, the system will rest in its stable focus for all times. Nevertheless a small excitation, e.g. by a stochastic forcing, can stimulate large loops in phase space (single spikes) before the system goes back to its fixed point [Fig. 2.3(b)]. This dynamical behaviour depicts the generation of action potentials in a neuron and excitable dynamics in general. Therefore this regime is called excitable regime. The additional unstable fixed

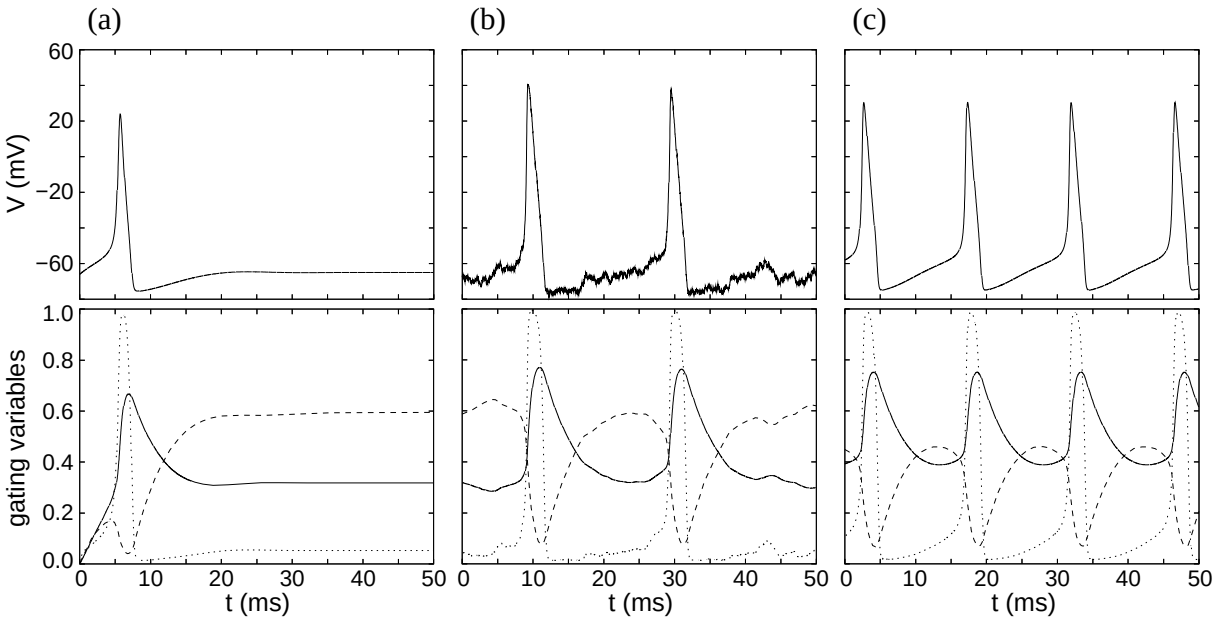


Figure 2.3. Time series of the Hodgkin-Huxley model [Eqs. (2.4)]. First row: The membrane potential $V(t)$. Second row: The gating variables, (—) $n(t)$, ($\cdot$ $\cdot$) $m(t)$, (- -) $h(t)$. (a), (b): Excitable regime $E1$ with $p = 0.125$ and $I = 0\mu A$, (a) without an external forcing, (b) with a weak stochastic forcing. (c): Oscillatory regime $O1$ with $p = 0.125$ and $I = 10\mu A$, without an external forcing.

points of the regime $E2$ do not change the temporal dynamics of the model compared to the regime $E1$ and thus the system in this regime also shows excitable dynamics.

As stated above the reduced Hodgkin-Huxley model allows an intuitive understanding of the excitable dynamics. First one has to calculate the nullclines of the system ($\dot{V} = 0$ and $\dot{n} = 0$), which are plotted in Fig. 2.4. The points of intersection of the nullclines are the fixed points of the system. The nullcline $\dot{V} = 0$ has two branches, one unstable and one stable branch. These branches are determined by the stability of the fixed points. For $I = 10\mu A$ and $p = 0.125$ [Fig. 2.4(a)] the only point of intersection lies on the unstable branch. The fixed point is thus unstable and the systems shows oscillatory dynamics. Decreasing the current $I$ an inverse Hopf bifurcation occurs and the fixed point moves to the stable branch of the nullcline. This is displayed in Fig. 2.4(b) for $I = 0\mu A$. The system is now in the excitable regime and a weak stochastic forcing, which has to exceed a certain threshold, can push the system in an area of the parameter space where $\dot{V} > 0$ forces the element to move to the right [Fig. 2.4(b)]. Following now the gradient $(\dot{V}, \dot{n})$ the system makes a large excursion through phase space before it moves back to the fixed point. The time series of $V(t)$ for such an excursion is displayed in Fig. 2.4(c) and one can clearly discern a single spike (action potential).

The HH model in the regimes $O1$ and $O2$ pictures the dynamic of an oscillatory neuron. The reason for such an oscillatory dynamics may be a permanent excitation induced by an external current, for example $I = 10\mu A$ for $p = 0.125$ [Figs. 2.2 and 2.4(a)].

In small areas of the parameter space, between the regimes with excitable ($E1$ and $E2$) and oscillatory ($O1$ and $O2$) dynamics, a stable focus and a stable limit cycle coexist in the regimes $O3$ and $O4$. A system in one of these regimes can either rest in its fixed point or it can show oscillatory dynamics. An external forcing, for example by noise, can induce

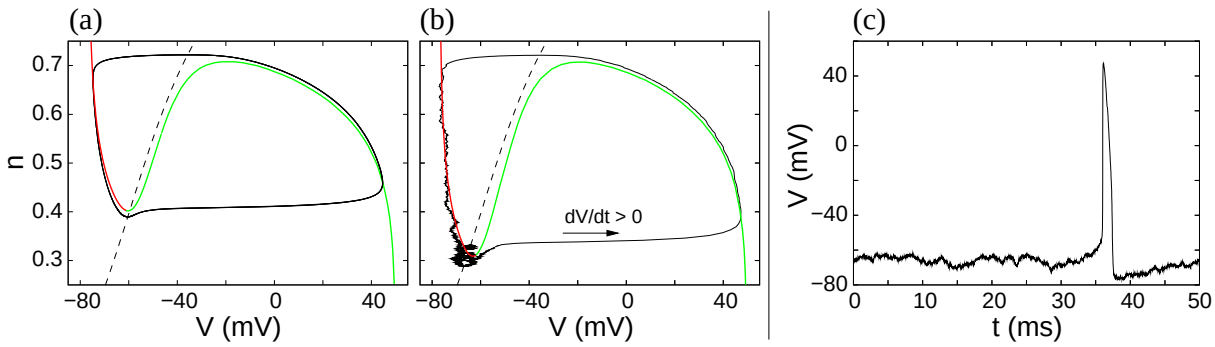


Figure 2.4. Nullclines and time series of the reduced Hodgkin-Huxley model [Eqs. (2.8)], (- -) nullcline $\dot{n} = 0$, (—) stable branch and (—) unstable branch of the nullcline $\dot{V} = 0$, (—) trajectory. (a): Trajectory in phase space for $I = 10\mu A$ and $p = 0.125$ (regime $O1$). (b), (c): Model dynamics for $I = 0\mu A$ and $p = 0.125$ (regime $E1$) with weak stochastic forcing, (b) trajectory in phase space, (c) time series of $V(t)$.

jumps between the two attractors. The probability to be in a certain area of attraction depends thereby on the size of the area of attraction and the strength of the external forcing.

The additional unstable fixed points found for the reduced model do not change the dynamics of the system qualitatively compared to the full model and thus $E2$ shows the same dynamics as $E1$, $O2$ shows the same dynamics as $O1$ and $O4$ shows the same dynamics as $O3$. Hence the reduced model approximates the dynamics of the full Hodgkin-Huxley model quiet well. Nevertheless the stability analysis reveals one difference between the models. The transition from the regimes $O3$ and $O4$ to $O1$ and $O2$ is shifted to smaller values of the parameter $p$ for the reduced model, and thus the regimes with coexisting stable limit cycle and stable focus are narrower.

## 2.2 FitzHugh-Nagumo Model

The FitzHugh-Nagumo (FHN) model is a frequently used standard model to describe excitable dynamics, but also oscillatory and bistable behaviour. It is a minimal model based on the reduced Hodgkin-Huxley model [Eqs. (2.8)], developed by FitzHugh 1961 [33] and Nagumo 1963 [34], where important groundwork was done by Bonhoeffer [32] (based on the Van-der Pol oscillator model). The model system consists of two coupled differential equations, which read:

$$\begin{aligned} \dot{u} &= \frac{1}{\epsilon}\left[u(1-u)(u-a) - v + d\right] \\ \dot{v} &= u - cv + e. \end{aligned} \tag{2.10}$$

In this minimal model $u(t)$ represents the fast relaxing membrane potential, while $v(t)$ mimics the slow potassium gating variable. The time scales of the variables are separated by the small parameter $\epsilon$, where $\epsilon = 0.01$ is used for the calculations in this thesis. The nonlinear voltage dependency of the Hodgkin-Huxley model is approximated by a cubic function in the fast variable and is linearised in the relevant region of the parameter space in the slow variable. The parameters $e$ and $c$ in the FHN model are results of this linearisation and have no direct counterpart in the Hodgkin-Huxley model.

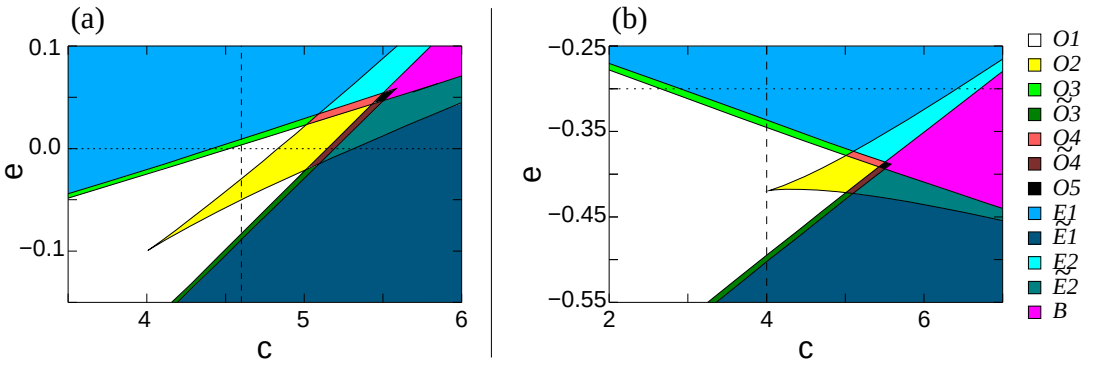


Figure 2.5. Stability analysis of the FitzHugh-Nagumo model [Eqs. (2.10)] in dependency on the parameters $c$ and $e$. (a): Parameter set 1 [Eq. (2.11)], (- -) $c = 4.6$, $(\cdot\ \cdot)$ $e = 0$. (b): Parameter set 2 [Eq. (2.12)], (- -) $c = 4$, $(\cdot\ \cdot)$ $e = -0.3$. (—) boundaries of the dynamical regimes. An explanation of the different dynamical regimes is given in the text.

### 2.2.1 Temporal Dynamics of the FitzHugh-Nagumo Model

The temporal dynamics of the FitzHugh-Nagumo model in dependency on the parameters $e$ and $c$ is studied in detail by means of a linear stability analysis for two different parameter sets. The result for parameter set 1

$$(\epsilon, a, d) = (0.01, 0.5, 0.1) \tag{2.11}$$

is displayed in Fig. 2.5(a) and the result for parameter set 2

$$(\epsilon, a, d) = (0.01, 0.5, 0.02) \tag{2.12}$$

in Fig. 2.5(b).

The overall structure of the result of the stability analysis is the same for both parameter sets. Changing the parameters $d$ and $a$ leads only to a shift and tilt of the diagram and thus corresponding regimes are found for different values of $e$ and $c$. Comparing the stability analysis of the FitzHugh-Nagumo model with the results for the Hodgkin-Huxley model one discerns two additional regimes:

- The bistable regime $B$: This dynamical regime has two stable foci which are separated by a saddle point.
- The regime $O5$: This regime is like $B$, but it has additionally three limit cycles. Each of the two stable foci is located in an unstable limit cycle. The unstable limit cycles and the saddle point are located in a stable limit cycle.

Since the regime $B$ is a bistable regime, an external stochastic forcing can induce jumps between the two attractors of this regime. With an additional weak signal one can observe stochastic resonance [37].

The reason for the emergence of the regimes $B$ and $O5$ is that $\dot{u} = 0$, the cubic nullcline, has, in difference to $\dot{V} = 0$ for the Hodgkin-Huxley model, two stable branches (symmetry of the model equations). In the following the stable branch found for smaller values of the variable $u$ is called lower stable branch and the other one upper stable branch of the cubic nullcline. In the case of three intersection points of the nullclines it is possible that two of them are stable [Fig. 2.6(a)].

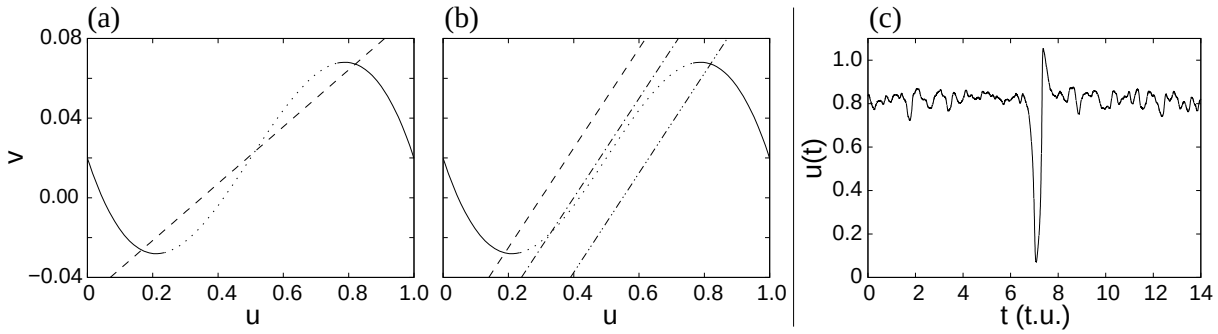


Figure 2.6. Nullclines and time series of the FitzHugh-Nagumo model [Eqs. (2.10)] for parameter set 2 [Eq. (2.12)]. (a), (b): (—) stable branches and (· ·) unstable branch of the cubic nullcline $\dot{u} = 0$. (a): (- -) linear nullcline $\dot{v} = 0$ for $e = -0.35$ and $c = 7$ (regime $B$). (b): linear nullclines $\dot{v} = 0$ for $c = 4$, (- -) $e = -0.3$ (regime $E1$), (- · -) $e = -0.4$ (regime $O1$), (- · · -) $e = -0.55$ (regime $\tilde{E}1$). (c): Time series $u(t)$ for $e = -0.55$ and $c = 4$ (regime $\tilde{E}1$) for a weak stochastic forcing.

The existence of the two stable branches of the cubic nullcline leads to a second important difference in the dynamics of the FitzHugh-Nagumo model compared to the dynamics of the Hodgkin-Huxley model. This difference is displayed in Fig. 2.6(b). Using parameterset 2 with $c = 4$ and $e = -0.3$ one is in the excitable regime $E1$ with a fixed point at the lower stable branch of the cubic nullcline. Decreasing the parameter $e$ the fixed point is moving to the unstable branch and for $e = -0.4$ one is in the regime $O1$. Decreasing the parameter value even further the fixed point moves to the upper stable branch. The dynamics of the system is now again excitable and a weak stochastic forcing can initiate large loops in phase space. The time series of the fast variable for such a spike is plotted in Fig. 2.6(c). In difference to the regime $E1$ the fixed point is found for a larger value of the variable $u$ and the loop in phase space leads to a reversed pulse. In a similar way one finds for all the regimes with only one stable fixed point, namely $E1$, $E2$, $O3$ and $O4$, corresponding regimes, where the fixed point is now at the upper stable branch of the cubic nullcline. To indicate that the stable fixed point is at the upper stable branch these regimes are marked with a tilde ($\tilde{E}1$, $\tilde{E}2$, $\tilde{O}3$ and $\tilde{O}4$ in Fig. 2.5).

### 2.2.2 General Classification of the Temporal Dynamics

Looking at the stability analysis of the model equations in the Figs. 2.2 and 2.5 one recognises three general types of temporal dynamics. The first is the excitable dynamics, which conflates the temporal behaviour found in the regimes $E1$ and $E2$. Regimes which allow excitable dynamics are denominated as $E$. For the FitzHugh-Nagumo model one additionally finds excitable regimes, where the stable focus is at the upper stable branch of the cubic nullcline ($\tilde{E}1$ and $\tilde{E}2$). To distinguish these regimes from $E$ they are denominated as $\tilde{E}$. The second important general type is the oscillatory dynamics, which is found in the regimes $O1$ and $O2$. In the following these oscillatory regimes are denominated as $O$. The third general type, the bistable dynamics, is found in the regime $B$. This regime does not represent a typical neuronal behaviour and can not be found in the Hodgkin-Huxley model.

The general classification $E$, $O$ and $B$ does not include all dynamical regimes found

for the FitzHugh-Nagumo and the Hogkin-Huxley model. In rather small areas of the parameter space one finds the additional regimes $O3$, $\tilde{O}3$, $O4$, $\tilde{O}4$ and $O5$. These regimes can show a more complex dynamics.

## 2.3 Net Dynamics

In this thesis the interplay of variability and noise is studied in spatially extended systems. These systems are nets of $N \times N$ coupled elements, where $N$ is the side length of the net. The single elements, which are labeled by the indices $1 \leq i, j \leq N$, are modeled by Eqs. (2.4), (2.8) and (2.10), respectively. The corresponding equations read

- for a net of Hodgkin-Huxley elements:

$$\begin{aligned}
\dot{V}_{ij} &= [I - G_{Na} m_{ij}^3 h_{ij}(V_{ij} - V_{Na}) - G_K n_{ij}^4 (V_{ij} - V_K) - G_L(V_{ij} - V_L)]/C + qK(V_{ij}) \\
\dot{n}_{ij} &= \alpha_n(V_{ij})(1 - n_{ij}) - \beta_n(V_{ij}) n_{ij} \\
\dot{m}_{ij} &= \alpha_m(V_{ij})(1 - m_{ij}) - \beta_m(V_{ij}) m_{ij} \\
\dot{h}_{ij} &= \alpha_h(V_{ij})(1 - h_{ij}) - \beta_h(V_{ij}) h_{ij},
\end{aligned} \tag{2.13}$$

- for a net of reduced Hodgkin-Huxley elements:

$$\begin{aligned}
\dot{V}_{ij} =& [I - G_{Na} m(V_{ij})^3 (0.8 - n_{ij})(V_{ij} - V_{Na}) \\
& - G_K n_{ij}^4 (V_{ij} - V_K) - G_L(V_{ij} - V_L)]/C + qK(V_{ij}) \\
\dot{n}_{ij} =& \alpha_n(V_{ij})(1 - n_{ij}) - \beta_n(V_{ij}) n_{ij},
\end{aligned} \tag{2.14}$$

- for a net of FitzHugh-Nagumo elements:

$$\begin{aligned}
\dot{u}_{ij} =& \frac{1}{\epsilon} [u_{ij}(1 - u_{ij})(u_{ij} - a) - v_{ij} + d] + qK(u_{ij}) \\
\dot{v}_{ij} =& u_{ij} - c v_{ij} + e.
\end{aligned} \tag{2.15}$$

$K(x_{ij})$, where $x_{ij}$ represents the fast variable $V$ or $u$ of the $ij$-th element at time $t$, denotes the coupling function and $q$ the coupling strength.

In this thesis two types of coupling are studied. The first is the global coupling with

$$K(x_{ij}) = \bar{x} - x_{ij}, \tag{2.16}$$

where $\bar{x}$ denotes the mean value of the fast variable of all elements (mean field):

$$\bar{x} = \frac{1}{N^2} \sum_{i,j=1}^{N} x_{ij}. \tag{2.17}$$

In order to study pattern formation and signal transmission through the net, the second type of the coupling is chosen to be a diffusive nearest-neighbour coupling, using a nine-point Laplacian for radial symmetry (eight neighbours):

$$\begin{aligned}
K(x_{ij}) =& \nabla^2 x_{ij}, \\
\nabla^2 x_{ij} =& \frac{1}{6\Delta h^2} [x_{i+1,j+1} + x_{i+1,j-1} + x_{i-1,j+1} + x_{i-1,j-1} \\
& + 4(x_{i+1,j} + x_{i-1,j} + x_{i,j+1} + x_{i,j-1}) - 20 x_{ij}].
\end{aligned} \tag{2.18}$$

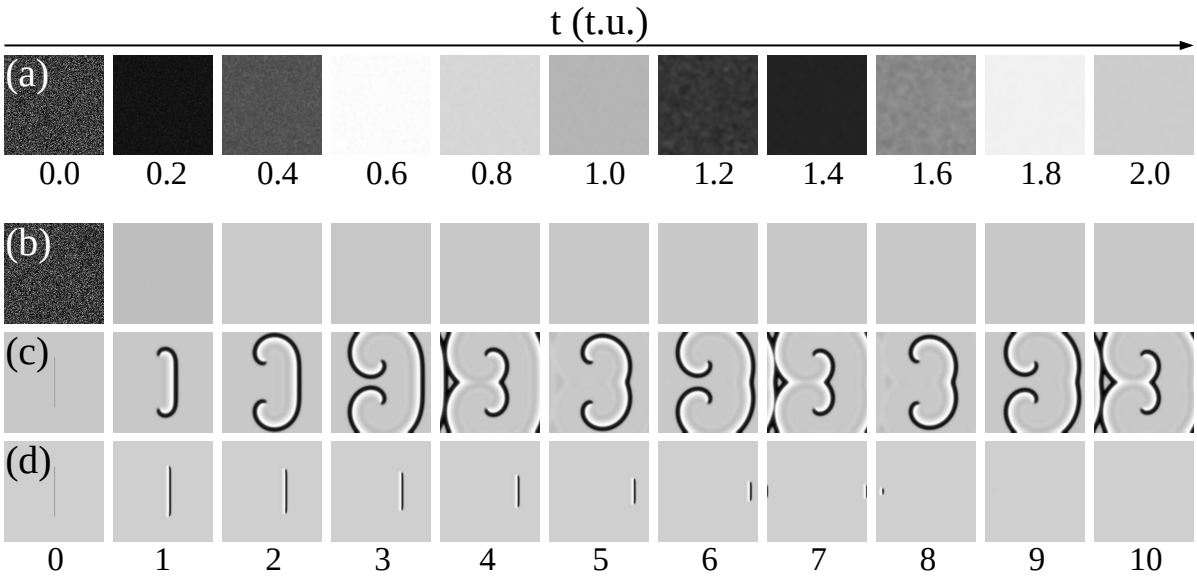


Figure 2.7. Snapshots of the fast variable of a net of FitzHugh-Nagumo elements [Eqs. (2.15)] with diffusive coupling [Eq. (2.18)] for parameter set 1 [Eq. (2.11)], $e = 0$, $N = 256$ and $q = 20$. The grey scale is explained in the text. (a): The oscillatory regime $O$ for $c = 4.6$, random initial conditions. (b), (c): The excitable regime $E_H$ for $c = 4.2$, (b) random initial conditions, (c) special initial conditions induce a spiral wave. (d): The subexcitable regime $E_S$ with $c = 3.5$, special initial conditions induce a spiral wave, which dies out.

The nets are integrated on a discrete spatial grid, where in the Chapters 4-6 and in Chapter 8 the boundaries are chosen to be periodic. In Chapter 7 Neumann (zero-flux) boundaries are used [8]. The spatial discretisation length $\Delta h$ from Eq. (2.18) is assumed to be one. This is roughly one order of magnitude smaller than the spatial extend of the smallest patterns studied in this thesis.

Without discussing the influence of the net size and the coupling strength in detail the most important pattern forming regimes of Eqs. (2.15) with diffusive coupling are displayed in Fig. 2.7. In this figure snapshots of the fast variable of a net of FHN elements are plotted in a linear grey scale, reaching from white for $u_{ij} \leq 0.0$ to black for $u_{ij} \geq 1.0$. All snapshots of nets of FHN elements plotted in this thesis are created using this grey scale.

If the single elements of the net are in the oscillatory regime $O$ they synchronise for nearly all initial conditions due to the coupling and, after a transient, one will find a synchronised oscillation [Fig. 2.7(a)]. The spatiotemporal oscillatory regime is as the temporal oscillatory regime denominated as $O$. The oscillatory net can also have stable wave train solutions, but they have a small area of attraction compared to the one for the synchronised oscillation. Starting with random initial conditions one will hardly ever find such wave train solutions.

If the elements in the net are in the excitable regime $E$ the spatially homogeneous and temporally constant solution is stable. Starting with random initial conditions in most cases one will find this trivial solution [Fig. 2.7(b)]. Nevertheless starting with special initial conditions excitation waves can be induced in the net, provided the net is large enough and the coupling is sufficiently strong. These waves can be wave fronts, circular

waves or spiral waves [Fig. 2.7(c)]. This pattern forming exitable regime is denominated as $E_H$. For nets, which consist of excitable elements, it is also possible that the only stable solution of the equations is the spatially homogeneous and temporally constant solution. All wave fronts die out after some time [Fig. 2.7(d)]. Consequently this regime, which is denominated as $E_S$, is called subexcitable.

For nets of HH and reduced HH elements [Eqs. (2.13) and (2.14)] one finds pattern forming regimes similar to the ones for the FHN model, which are likewise denominated as $O$, $E_H$ and $E_S$.

## 2.4 Data Analysis

To study the dynamics of spatially extended systems one needs some analysis tools, which are briefly introduced in the following subsections. They allow to study synchronisation [35], transitions between dynamical regimes [10, 38] and pattern formation [8, 39].

### 2.4.1 Time Averaged Mean Field

To identify a transition from the oscillatory net dynamics $O$ to the excitable regime $E_H$, where all elements rest in their fixed points, the time averaged mean field $M$, which is defined as

$$M = \langle \bar{x}(t) \rangle_T, \tag{2.19}$$

is used as an oder parameter. In this equation $\bar{x}(t)$ is the mean-field of the variable $x(t)$ at time $t$ [Eq. (2.17)] and the brackets $\langle .. \rangle_T$ denote the time average over the total integration time $T$, where the transients have to be excluded. A transition from oscillatory to excitable dynamics is associated with a jump of the time averaged mean field $M$ to much smaller values [38].

### 2.4.2 Relative Resting Time

To distinguish excitable from oscillatory and subexcitable dynamics the relative resting time $T_r$ is used. An element in the net is excitable, if it is in a special confined phase space area close to the fixed point. For the FitzHugh-Nagumo model with parameter set 1 [Eq. (2.11)] the borders of this area are given for example by $u_{ij} < 0.35$ and $v_{ij} < 0.1$. The relative resting time measures the average time the elements of a net are in this area of the phase space divided by the total integration time $T$:

$$T_r = \frac{1}{N^2} \sum_{i,j=1}^{N} \frac{t_{ij}}{T}, \tag{2.20}$$

where $t_{ij}$ is the time the $ij$-th element rests in the confined phase space area. The net is assumed to be excitable if $T_r > 0.98$ [10, 11, 38].

### 2.4.3 Order Parameter $R$

To characterise the synchronisation of the elements in the net the order parameter $R$ [35, 40] is used. This quantity is defined as the ratio of the standard deviation of the

mean-field $\bar{x}$ [Eq. (2.17)] to the standard deviation of the single element time series $x_{ij}$ averaged over $i$ and $j$:

$$R = \frac{\langle \bar{x}^2 \rangle_T - \langle \bar{x} \rangle_T^2}{\frac{1}{N^2} \sum_{i,j=1}^{N} \left( \langle x_{ij}^2 \rangle_T - \langle x_{ij} \rangle_T^2 \right)}. \tag{2.21}$$

The brackets $\langle .. \rangle_T$ denote the time average over the total integration time $T$, where the transients have to be excluded. In this thesis the order parameter $R$ is always calculated for the fast variable of the model equations.

If all elements oscillate completely synchronised $R$ will take its maximum value $R = 1$. In the totally unsynchronised situation one finds the minimal value $R = 0$. In general one can state that a higher value of $R$ indicates a better synchronisation.

### 2.4.4 Spatial Cross Correlation

To quantify the coherence of the pattern formation in diffusively coupled nets the spatial cross correlation $S$ is used [8, 39]. It is defined as the space and time averaged nearest-neighbour amplitude-distance $A(t)$ of all elements (spatial autocovariance) normalised by the total spatial amplitude variance $V_a(t)$, which is defined as

$$V_a(t) = \frac{1}{N^2} \sum_{i,j=1}^{N} (x_{ij} - \bar{x})^2. \tag{2.22}$$

The spatial autocovariance of the nearest-neighbours can be written as

$$A(t) = \frac{1}{N^2} \sum_{i,j=1}^{N} \frac{1}{\aleph} \sum_{k=1}^{\aleph} (x_{ij} - \bar{x})(x_k - \bar{x}), \tag{2.23}$$

with the index $k$, summing up all $\aleph = 4$ elements of a von Neumann neighbourhood at each lattice site $ij$, and the mean-field $\bar{x}$ [Eq. (2.17)]. The spatial cross correlation is given by

$$S = \left\langle \frac{A(t)}{V_a(t)} \right\rangle_T. \tag{2.24}$$

The brackets $\langle .. \rangle_T$ denote the time average over the total integration time $T$, where the transients have to be excluded. $S$ is a measure for the relative change of the local order and thus for the coherence of the patterns found in spatially extended system.

If the net exhibits a completely coherent dynamics in space and time one gets the maximum value $S = 1$. For a completely asynchronous net dynamics one receives $S = 0$ and for a strong anti-correlated dynamics the spatial cross correlation takes up a minimum value of minus one.

# 3 Variability and Noise

In the last decades it was shown that noise, which denotes a fast stochastic process, may strongly influence the dynamics of many nonlinear systems. Examples are: Stochastic resonance [37], spatiotemporal stochastic resonance [3, 7, 8], noise-induced phase transitions [11, 13] and coherence resonance [9]. Noise may enhance the phase synchronisation in excitable media [41] and may lead to a synchronised firing of FitzHugh-Nagumo neurons [42]. Furthermore noise strongly affects the synchronisation in oscillatory [43] and chaotic systems [44].

In contrast to noise, internal variability (diversity, heterogeneity) denotes static stochastic differences between otherwise equal elements. Such differences do often effect spatiotemporal dynamics. The influence of parameter variability on the synchronisation of coupled oscillators was investigated by Winfree [18] and Kuramoto [19]. These results are the basis for most of the studies on synchronisation even today [45]. The effect of variability on spatiotemporal chaos was observed in [20, 21]. Furthermore variability can play an important role for pattern formation in a net of biochemical oscillators [22]. Recently it was demonstrated, that diversity can cause resonance-like phenomena in networks of nonlinear elements [23, 24].

Lately the existence of variability in populations of bacteria has been confirmed experimentally [17] and one assumes that both, noise and variability, are omnipresent in biological systems. The interplay of these stochastic quantities may have an essential influence on spatiotemporal dynamics and pattern formation.

In this chapter the properties of variability and noise are briefly introduced and the stochastic terms are implemented in the model equations [Eqs. (2.13), (2.14) and (2.15)]. Furthermore the difference between additive and multiplicative stochastic terms is explained. Multiplicative variability and multiplicative noise may have a systematic influence on the model systems and methods to theoretically predict this influence are shortly presented.

## 3.1 Modelling Variability and Noise

The noise term $\xi_n(t)$ is a fast stochastic process, which is characterised by its probability distribution, its moments and its correlation function [8, 13]. Because of the central limit theorem the probability distribution is often assumed to be Gaussian. In this case all but the first two moments, the mean value and the variance, of the stochastic process vanish. The variance $\sigma_n^2$ of the Gaussian distribution $P(\xi_n, \sigma_n)$ can be defined as the noise intensity and $\sigma_n$ as the noise strength. A second approximation can be done if the time and length scales of the noise are much smaller than the relevant scales of the dynamics of the observed system. In this case the noise is assumed to be white in space and time and the corresponding correlation function is a $\delta$-distribution [13].

In contrast to noise variability denotes static stochastic differences between the otherwise equal elements of a system. This means that a model parameter may stochastically

change its values from element to element. These fixed parameter values can again be characterised by a Gaussian probability distribution, where $\sigma_v^2$, the variance of the Gaussian distribution, denotes the variability intensity and $\sigma_v$ the variability strength. If the correlation length of the variability is small compared to the relevant length scales of the system one can again assume that the static stochastic differences are uncorrelated in space and the spatial correlation is hence given by a $\delta$-distribution [13].

If the correlation length and/or the correlation time of a stochastic process is at least of the order of a relevant length and/or time scale of the system dynamics one has to assume a more complex correlation function with a finite correlation length and/or time. A stochastic term with such a correlation is denoted as coloured in space and/or time. Examples are the exponential correlation and the $1/f^{\alpha}$-correlation [13]. The influence of noise, with corresponding correlation functions, has been studied in detail. It was shown that the correlation time and length of a stochastic process may have a strong influence on nonlinear systems [46, 47, 48, 49, 50]. Furthermore, the correlation of a noise term may influence the pattern formation in subexcitable media (STSR) [8] and noise induced transitions [11].

All stochastic processes, studied in this thesis, are characterised by Gaussian probability distributions. Thereby all noise terms are assumed to be white in space and time. The reason for this simplification is that for the fundamental studies of the interplay of noise and variability presented in this thesis the simplest case is chosen. Furthermore, coloured noise, both additive and multiplicative, has already been studied in-depth in excitable and oscillatory nets [8, 11]. However the interplay of variability and coloured noise may be of interest for further studies. Coloured variability was, to the best of my knowledge, never studied in diffusively coupled oscillatory or excitable nets before and thus, besides white variability, the influence of the spatial correlation of the variability is investigated in Chapter 7.

A given net with variability is not completely determined by the value of the variability strength. A special realisation of the net will never be like the other, but in general all realisations of a large net for a given variability strength should show a similar dynamical behaviour. This means that if a special realisation of a net for a certain value of $\sigma_v$ exhibits pattern formation one expects to find this behaviour for other realisations of the net for this value of the variability strength as well. However the shape of the patterns will be slightly different for each realisation.

For the simulation of stochastic processes on the computer one first creates equally distributed pseudo-random numbers. In this thesis this is done with the random number generator Mersenne Twister [51, 8]. To simulate Gaussian distributed random processes the Box-Müller-Wiener algorithm, which generates two Gaussian distributed random numbers from two equally distributed ones, is applied [13]. To get variability with a finite correlation in space from the Gaussian random numbers a frequency filtering methods is used [8, 13].

To study the influence of the fluctuations on the systems dynamics in detail the stochastic model equations have to be integrated numerically. In this thesis the nets are integrated on a discrete spatial grid with the spatial discretisation length $\Delta h = 1$ (Chapter 2). The time integration of the stochastic differential equations is done using a Heun method [13]. The time steps for the integration of the FHN model are chosen to be $\Delta t = 0.001$ $t.u.$, where one $t.u.$ accords approximately with the oscillation period of the net in the regime $O$. The integration of the HH model is done with time steps of the length $\Delta t = 0.001$ $ms$.

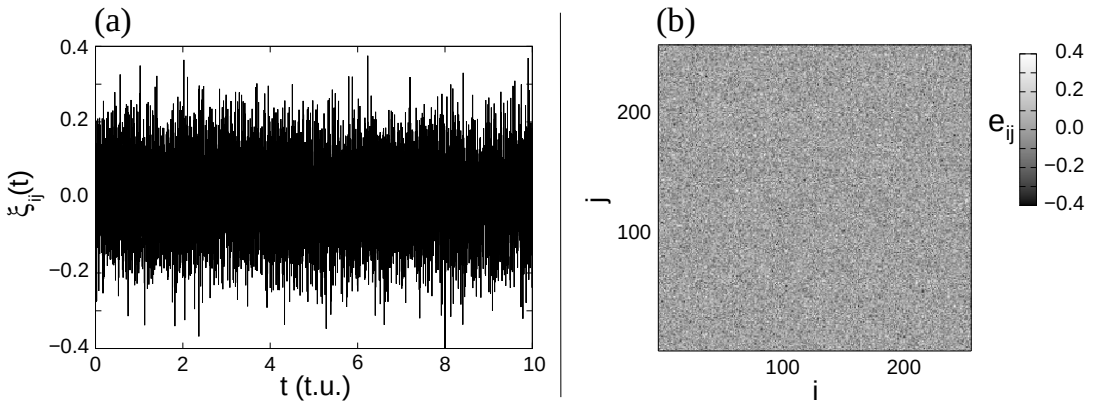


Figure 3.1. (a): Time series $\xi_{ij}(t)$ of white additive noise [correlation function Eqs. (3.5)] for the $ij$-th grid point, $\sigma_{n,e} = 0.1$. (b): The spatial distribution of the parameter values $e_{ij}$ for white variability [correlation function Eqs. (3.3)], $\mathfrak{E} = 0$, $N = 256$ and $\sigma_{v,e} = 0.1$.

## 3.2 Variability and Noise in Nets of FitzHugh-Nagumo Elements

The model equations for a net of FitzHugh-Nagumo elements with noise and variability read:

$$\begin{aligned} \dot{u}_{ij} =& \frac{1}{\epsilon}\left[u_{ij}(1-u_{ij})(u_{ij}-a) - v_{ij} + d\right] + qK(u_{ij}) \\ \dot{v}_{ij} =& u_{ij} - c_{ij}[1+\eta_{ij}(t)]v_{ij} + e_{ij} + \xi_{ij}(t). \end{aligned} \tag{3.1}$$

In this thesis only variability in the parameters $c$ and $e$ of the slow variable $v(t)$ is considered. In the following the variability in the parameter $e$ is called additive variability, because this parameter is an additive term in the differential equation. This is different for the parameter $c$, which is multiplied with the system variable $v$. Hence the variability in this parameter is called multiplicative variability. Due to the variability the values $c_{ij}$ and $e_{ij}$ of the parameters $c$ and $e$ can change from element to element. The parameter values are Gaussian distributed numbers and the parameters $\mathfrak{E}$ and $C$, with

$$\langle e_{ij}\rangle = \mathfrak{E},\ \langle c_{ij}\rangle = C, \tag{3.2}$$

are the mean values of the Gaussian distributions $P(e, \sigma_{v,e})$ and $P(c, \sigma_{v,c})$, respectively. The standard deviation $\sigma_{v,e}$ defines the strength of the additive variability and the standard deviation $\sigma_{v,c}$ the strength of the multiplicative variability.

In this thesis two types of spatial correlation of the variability are studied. In the Chapters 4-6 the variability is considered to be white in space (white variability). In this case the correlation functions are given by $\delta$-distributions:

$$\begin{aligned} \langle (e_{ij} - \mathfrak{E})(e_{kl} - \mathfrak{E})\rangle &= \sigma^2_{v,e}\delta_{ij,kl} \\ \langle (c_{ij} - C)(c_{kl} - C)\rangle &= \sigma^2_{v,c}\delta_{ij,kl}. \end{aligned} \tag{3.3}$$

This means that the parameter values $e_{ij}$ and $c_{ij}$ of the $ij$-th element in the net are completely independent of the corresponding values of the neighbour elements [Fig. 3.1(b)].

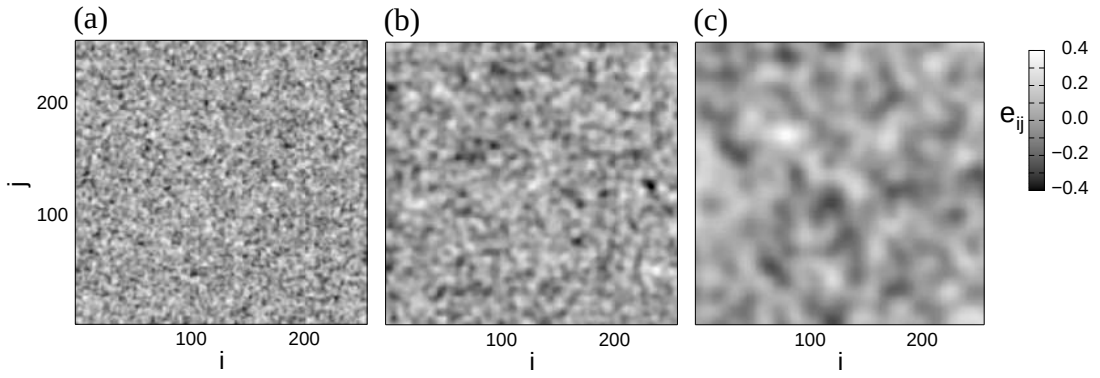


Figure 3.2. The spatial distribution of the parameter values $e_{ij}$ of the FHN model for exponentially correlated variability [correlation function Eqs. (3.4)], $\mathfrak{E} = 0$, $N = 256$ and $\sigma_{v,e} = 0.1$. (a): $\lambda_{v,e} = 1$. (b): $\lambda_{v,e} = 2$. (c): $\lambda_{v,e} = 5$.

The second type of spatial correlation of the variability, which is used in Chapter 7, is the exponential correlation, where the correlation functions read:

$$\begin{aligned} \langle (e_{ij} - \mathfrak{E})(e_{kl} - \mathfrak{E}) \rangle &= \sigma_{v,e}^2 exp\left( \frac{-[(i-k)^2 + (j-l)^2]}{\lambda_{v,e}^2} \right) \\ \langle (c_{ij} - C)(c_{kl} - C) \rangle &= \sigma_{v,c}^2 exp\left( \frac{-[(i-k)^2 + (j-l)^2]}{\lambda_{v,c}^2} \right). \end{aligned} \tag{3.4}$$

The variability is now characterised by the variability strength and additionally by the correlation length, where $\lambda_{v,e}$ is the correlation length of the additive variability and $\lambda_{v,c}$ the correlation length of the multiplicative variability. The correlation length measures the spatial range of the correlation and with growing $\lambda$ larger clusters of elements with similar parameter values occur in the net [13, 8]. This is demonstrated in Fig. 3.2 for the additive variability using three different values of $\lambda_{v,e}$.

For exponentially correlated variability one finds rather smooth spatial parameter distributions for large correlation lengths, for instance $\lambda_{v,e} = 5$ in Fig. 3.2(c). This is different for the spatial $1/f^{\alpha}$-correlation, an other possible choice of the spatial correlation of the variability. In this case one finds cloudy structures with fractal properties [8]. This difference does however not change the net dynamics qualitatively. For the simulations with exponentially correlated variability presented in this thesis one finds similar results for $1/f^{\alpha}$-correlated variability.

One can also consider variability in the parameters $d$ and $a$ of the model equations. Variability in $d$ would be additive variability, like the variability in $e$, and all the results presented in this thesis for additive variability can also be obtained for variability in parameter $d$. It is thus sufficient to study additive variability only in one variable. The multiplicative variability is chosen to be in parameter $c$ because this case is easier to handle than the variability in parameter $a$. Changing the value of $c$ just leads to a tilt of the linear nullcline and thus to a change of its gradient angle. This fact leads to an easy analytical approximation of the influence of the variability in $c$ on the net dynamics, as can be seen in the next subsection. Till now there is no experimental evidence in which model parameters the variability might play an important role and thus, for the general study of the possible influences of the multiplicative variability presented in this thesis, the simplest case is chosen. Nevertheless for further studies it might be of interest to

study variability in parameter $a$.

The noise terms $\xi_{ij}(t)$ and $\eta_{ij}(t)$ in Eqs. (3.1) are taken to be zero mean spatially uncorrelated Gaussian white noise [Fig. 3.1(a)]. Hence the correlation functions read:

$$\begin{aligned}\langle \xi_{ij}(t)\xi_{kl}(t')\rangle &= \sigma_{n,e}^2 \delta_{ij,kl}\delta(t-t') \\ \langle \eta_{ij}(t)\eta_{kl}(t')\rangle &= \sigma_{n,c}^2 \delta_{ij,kl}\delta(t-t').\end{aligned} \tag{3.5}$$

The white additive noise $\xi_{ij}(t)$ is studied in $\dot{v}(t)$ of Eqs. (3.1), as it is done in most publications. However one does not find different results for additive noise in the fast variable of the model system. The noise in parameter $c$ is, like the variability in this parameter, a multiplicative stochastic term. The reason to study the multiplicative noise in parameter $c$ and not in parameter $a$ in the fast variable is, as for the multiplicative variability, that it is much easier to handle. Beyond that multiplicative noise in the slow variable of neuronal models is already discusses in the literature [10, 11] and this thesis aims to extend these results.

There is a qualitative difference between the additive and the multiplicative stochastic terms. Multiplicative noise and multiplicative variability may have a systematic influence on the system dynamics [13], this is demonstrated in the following subsections. The additive noise and the additive variability do not have a similar influence and the results presented in this thesis concerning the additive stochastic terms are based on numerical simulations only.

### 3.2.1 The Effective Parameter $\langle c \rangle$

Multiplicative noise has a systematic influence on the dynamics of a net of FHN elements. This can be shown when a small noise expansion [13] is applied to Eqs. (3.1). The first order of this expansion results in deterministic equations, which read:

$$\begin{aligned}\dot{u}_{ij} =& \frac{1}{\epsilon}\left[u_{ij}(1-u_{ij})(u_{ij}-a) - v_{ij} + d_u\right] + qK(u_{ij}) \\ \dot{v}_{ij} =& u_{ij} - c_{ij}(1 - \frac{1}{2}\sigma_{n,c}^2 c_{ij})v_{ij} + e_{ij}.\end{aligned} \tag{3.6}$$

The systematic influence of the multiplicative noise is given by the deterministic term $-\frac{1}{2}\sigma_{n,c}^2 c_{ij}$, whereas the additive noise terms $\xi_{ij}(t)$ does completely vanish in this approximation. This result shows that the parameter $\sigma_{n,c}$ systematically changes the gradient angle $\alpha$ of the linear nullcline ($\dot{v}=0$):

$$\alpha(c,\sigma_{n,c}) = \arctan\left((c - \frac{1}{2}\sigma_{n,c}^2 c^2)^{-1}\right). \tag{3.7}$$

Increasing the noise strength tilts the linear nullclines to the left. Thus the multiplicative noise can completely change the dynamics of a net of FitzHugh-Nagumo elements [10, 11].

The variability in parameter $c$ does act in a different way. Nevertheless it also has a systematic influence on the net dynamics, which can be seen calculating the mean gradient angle of the linear nullcline $\langle\alpha\rangle$. This macroscopic net parameter is given by

$$\langle\alpha\rangle = \frac{1}{N^2}\sum_{i,j=1}^{N}\alpha(c_{ij},\sigma_{n,c}) \tag{3.8}$$

and can be calculated approximately for a large net:

$$\langle\alpha\rangle \approx \langle\alpha\rangle(\sigma_{n,c}, \sigma_{v,c}) = \int_{-\infty}^{\infty} \alpha(c, \sigma_{n,c}) P(c, \sigma_{v,c}) dc \; . \tag{3.9}$$

One finds that the mean gradient angle of the net depends on the noise strength $\sigma_{n,c}$ and the variability strength $\sigma_{v,c}$.

Using Eq. (3.9) one can calculate the mean value of parameter $c$, the effective parameter $\langle c\rangle$, in dependency on $\sigma_{n,c}$ and $\sigma_{v,c}$:

$$\langle c\rangle(\sigma_{n,c}, \sigma_{v,c}) = \frac{1}{\tan[\langle\alpha\rangle(\sigma_{n,c}, \sigma_{v,c})]}. \tag{3.10}$$

Comparing the value of $\langle c\rangle$ with the results of the stability analysis in dependency on parameter $c$ presented in Fig. 2.5 one can predict the dynamics of the net. Thus Eq. (3.10) yields an easy deterministic approximation of the systematic influence of the variability and the noise in parameter $c$ on the net dynamics. However it does neglect the influence of the net size and the coupling strength. How good this approximation works, and for which net parameters $N$ and $q$ it is valid, is investigated in the following chapters.

### 3.2.2 The Mean Field Approximation

A second possibility to approximate the influence of variability on large nets is the mean field approximation [52, 53]. For a net of FHN elements [Eqs. (3.1)], neglecting the noise terms ($\sigma_{n,e} = 0$ and $\sigma_{n,c} = 0$), one gets the following equations after some lengthy calculations:

$$\begin{aligned}
\dot{\bar{u}} &= [\bar{u}(1-\bar{u})(\bar{u}-a) - \bar{v} + d]/\epsilon \\
\dot{\bar{v}} &= \bar{u} - C\bar{v} + \mathfrak{E} - W_v \\
\dot{W}_u &= \{[-3\bar{u}^2 + 2(a+1)\bar{u} - a]/\epsilon - q\}W_u - W_v/\epsilon \\
\dot{W}_v &= -\sigma_{v,c}^2 \bar{v} + W_u - CW_v.
\end{aligned} \tag{3.11}$$

The variable $\bar{u}$ is thereby the mean field of $u$ and $\bar{v}$ the mean field of $v$ [Eq. (2.17)]. The variables $W_u(t)$ and $W_v(t)$ are the shape parameters, which describe the influence of the variability and the coupling strength on the system dynamics. One sees that Eqs. (3.11) do not depend on $\sigma_{v,e}$, and thus the additive variability has no systematic influence on the net dynamics. The advantage of Eqs. (3.11) compared with Eq. (3.10) is that it does not neglect the coupling strength $q$, which remains as a parameter in the approximation.

To analyse the influence of $\sigma_{v,c}$ and the coupling strength $q$ on the net dynamics a stability analysis in dependency on these two parameters can be applied to Eqs. (3.11). In Chapter 4 such a stability analysis is presented and its results are compared with numerical simulations.

## 3.3 Variability and Noise in Nets of Hodgkin-Huxley Elements

The equations of a net of Hodgkin-Huxley elements [Eqs. (2.13)] with noise and variability read:

$$\begin{aligned}
\dot{V}_{ij} &= [I_{ij} - G_{Na} m_{ij}^3 h_{ij}(V_{ij} - V_{Na}) - G_K n_{ij}^4 (V_{ij} - V_K) - G_L(V_{ij} - V_L) + \xi'_{ij}(t)]/C \\
&\quad + qK(V_{ij}) \\
\dot{n}_{ij} &= \alpha_n(V_{ij})(1 - n_{ij}) - \beta_{n,ij}(V_{ij}) n_{ij} \\
\dot{m}_{ij} &= \alpha_m(V_{ij})(1 - m_{ij}) - \beta_m(V_{ij}) m_{ij} \\
\dot{h}_{ij} &= \alpha_h(V_{ij})(1 - h_{ij}) - \beta_h(V_{ij}) h_{ij},
\end{aligned} \tag{3.12}$$

where

$$\beta_{n,ij}(V_{ij}) = p_{ij}[1 + \eta'_{ij}(t)] \exp[-(V_{ij} + 65)/80]. \tag{3.13}$$

For a corresponding net of reduced Hodgkin-Huxley [Eqs. (2.14)] elements one gets the following equations:

$$\begin{aligned}
\dot{V}_{ij} =& [I_{ij} - G_{Na} m(V_{ij})^3 (0.8 - n_{ij})(V_{ij} - V_{Na}) \\
& - G_K n_{ij}^4 (V_{ij} - V_K) - G_L(V_{ij} - V_L) + \xi'_{ij}(t)]/C + qK(V_{ij}) \\
\dot{n}_{ij} =& \alpha_n(V_{ij})(1 - n_{ij}) - \beta_{n,ij}(V_{ij}) n_{ij}.
\end{aligned} \tag{3.14}$$

The variability, which is considered to be white, is introduced in the parameters $I$ and $p$. Hence the corresponding parameter values $p_{ij}$ and $I_{ij}$ are Gaussian distributed numbers, with

$$\begin{aligned}
\langle I_{ij} \rangle &= \Im, \ \langle (I_{ij} - \Im)(I_{kl} - \Im) \rangle = \sigma_{v,I}^2 \delta_{ij,kl} \\
\langle p_{ij} \rangle &= \Pi, \ \langle (p_{ij} - \Pi)(p_{kl} - \Pi) \rangle = \sigma_{v,p}^2 \delta_{ij,kl}.
\end{aligned} \tag{3.15}$$

The variability in parameter $I$ is additive variability, where $\Im$ is the mean value of the distribution $P(I, \sigma_{v,I})$ and $\sigma_{v,I}$ is the strength of the additive variability. The current $I$ is easy to measure in experiments with real neurons and one can control the current from the outside, for example with an electrode. The additive variability is introduced in this parameter in the hope that corresponding experimental results may be availabe in the future. The variability in parameter $p$ is multiplicative variability, where $\Pi$ is the mean value of the distribution $P(p, \sigma_{v,p})$ and $\sigma_{v,p}$ is the strength of the multiplicative variability. Multiplicative variability can also be introduced in other model parameters, but, without having further evidence in which parameter multiplicative variability might be important, the parameter $p$ is chosen in this thesis, because this parameter has a strong influence on the dynamics of the HH model (Fig. 2.2).

The noise terms $\xi'_{ij}(t)$ and $\eta'_{ij}(t)$ are considered to be zero mean spatially uncorrelated Gaussian white noise and thus their correlation functions read:

$$\begin{aligned}
\langle \xi'_{ij}(t) \xi'_{kl}(t') \rangle &= \sigma_{n,I}^2 \delta_{ij,kl} \delta(t - t') \\
\langle \eta'_{ij}(t) \eta'_{kl}(t') \rangle &= \sigma_{n,p}^2 \delta_{ij,kl} \delta(t - t').
\end{aligned} \tag{3.16}$$

The additive noise $\xi'_{ij}(t)$ is, as the additive variability, implemented in the first equation of the HH model. This stochastic term can be interpreted as a fast stochastically fluctuating current. The multiplicative variability and the multiplicative noise are introduced in

parameter $p$ of the model equations, because noise in this parameter strongly influences the net dynamics. Nevertheless multiplicative noise and multiplicative variability in other model parameters might be an interesting subject for further studies, especially when adequate experimental results are available.

As stated above the multiplicative stochastic terms may have a systematic influence on the system dynamics. A method to predict this influence for the multiplicative noise in parameter $p$ of the HH model is presented in the next subsection, however one does not have a simple method to predict the systematic influence of the multiplicative variability in this case.

### 3.3.1 The Small Noise Expansion

Applying a small noise expansion [13] the first order of this expansion provides a deterministic approximation of the second equation of Eqs. (3.12) and Eqs. (3.14) in dependency on the noise strength $\sigma_{n,p}$. Neglecting the variability ($I_{ij} = I$, $p_{ij} = p$ and $\beta_{n,ij} = \beta_n$), the additive noise term vanishes (additive noise has no systematic influence on the net dynamics) and the resulting deterministic equation for the temporal change of the gating variable $n$ reads:

$$\dot{n}_{ij} = \alpha_n(V_{ij})(1 - n_{ij}) - \left(\beta_n(V_{ij}) - \frac{1}{2}\sigma_{n,p}^2\beta_n^2(V_{ij})\right) n_{ij}. \tag{3.17}$$

Analysing the deterministic equations of a net of HH elements obtained from Eqs. (3.12) and Eq. (3.17) by applying a linear stability analysis the systematic influence of the multiplicative noise can be predicted. The same procedure can be done for the small noise expansion of a net of reduced HH elements obtained from Eqs. (3.14) and Eq. (3.17). Corresponding stability analyses are performed in Chapter 6 and their results are compared with numerical simulations.

For the multiplicative variability in the HH equations one does not find an easy approximation like the mean gradient angle for the FHN system. One can calculate a mean field approximation, as in Section 3.2.2, but one receives for the full model eight and for the reduced model four highly nonlinear differential equations. These equations do not yield an instructive description of the influence of the variability and to analyse their dynamics one has to perform a costly numerical stability analysis. Therefore the systematic influence of the multiplicative variability in parameter $p$ is demonstrated in Chapter 6 by directly integrating the stochastic model equations.

# 4 Variability and Noise in Oscillatory Nets of FitzHugh-Nagumo Elements

In the last years it was shown that noise and variability may have a strong influence on the dynamics of oscillatory spatially extended systems. The stochastic terms affect the synchronisation of oscillatory media [19, 43] and variability can induce pattern formation in chains of chemical oscillators [22].

Oscillatory dynamics is found in many biological systems. Metabolic processes show oscillatory dynamics in yeast [54, 55] and may act as a circadian clock in prokaryotes [56]. A completely different example is the dynamics of foodwebs, which can be oscillatory, and even chaotic [57]. Oscillatory dynamics is also of relevance for neuronal systems. Pathological cerebral synchronised oscillations are able to perturb normal brain functions. This behaviour plays an important role for some neural diseases like Parkinson's disease or essential tremor [58]. In this context, it is important to find methods to suppress undesirable global oscillations in neural networks [58, 59, 60, 61]. One method, which leads not only to a suppression of these unwanted oscillations, but also to the restoration of excitable dynamics has been presented in [10], where multiplicative noise was used to stabilise the deterministically unstable fixed point in an array of oscillatory systems. This noise induced excitability (NIE) was also reported in nets of FitzHugh-Nagumo elements with coloured multiplicative noise [11].

Throughout this chapter oscillatory nets of FitzHugh-Nagumo elements [Eqs. (3.1)] with white variability [Eqs. (3.3)] are studied, where parameter set 1 [Eq. (2.11)] is used [38, 40]. The corresponding stability analysis for a single FitzHugh-Nagumo element in dependency on the parameters $e$ and $c$ is presented in Fig. 2.5(a). The mean values $\mathfrak{E}$ and $C$ of the probability distributions from Eqs. (3.2) are chosen to be

$$(\mathfrak{E}, C) = (0, 4.6). \tag{4.1}$$

Without variability each FHN element has the same parameter values $e_{ij} = \mathfrak{E}$ and $c_{ij} = C$. In this case, according to the stability analysis the elements are in the regime $O$ and without noise they perform autonomous limit cycle oscillations. The nets studied in this chapter are thus oscillatory and yield, due to the coupling ($q > 0$), a synchronised output (global oscillation) after a transient for nearly all initial conditions [Fig. 2.7(a)].

## 4.1 Additive Variability and Additive Noise

Throughout this section the influence of additive noise and white additive variability on oscillatory nets of diffusively coupled FitzHugh-Nagumo elements [Eqs. (3.1) and (2.18)] is studied, while multiplicative stochastic influences are neglected ($\sigma_{n,c} = 0$ and $\sigma_{v,c} = 0$). The numerical simulations are done varying the side length $N$, the coupling strength $q$, the noise strength $\sigma_{n,e}$ and the variability strength $\sigma_{v,e}$.

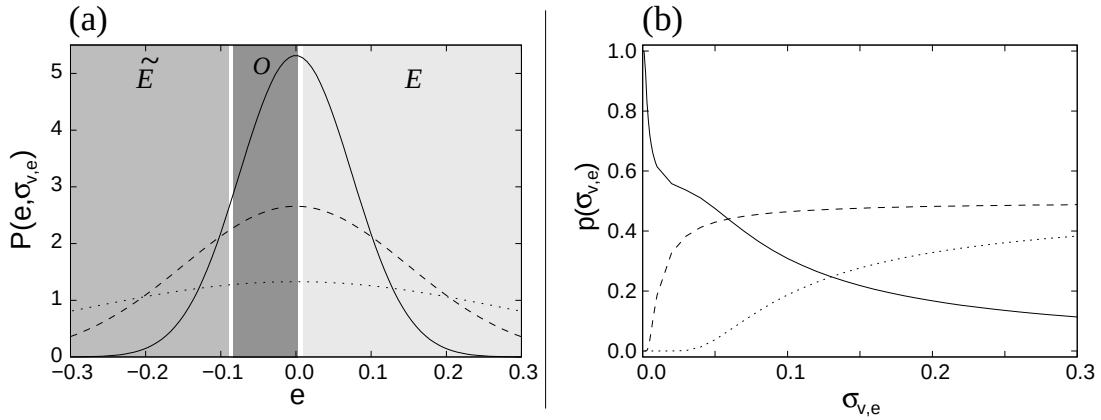


Figure 4.1. (a): The Gaussian probability distribution $P(e, \sigma_{v,e})$ for three different values of the variability strength, (—) $\sigma_{v,e} = 0.075$, (- -) $\sigma_{v,e} = 0.15$ and (· ·) $\sigma_{v,e} = 0.3$. The grey areas mark the dynamical regimes. (b): Probability $p(\sigma_{v,e})$ for one FitzHugh-Nagumo element to be in the oscillatory regime $O$ (—), the excitable regime $E$ (- -) and the excitable regime $\tilde{E}$ (· ·) in dependency on the variability strength $\sigma_{v,e}$.

The dynamics of a single FHN element strongly depends on its parameter value $e_{ij}$ [Fig. 2.5(a)]. For $e_{ij} > 0.009$ the element is in the excitable regime $E$ and a small excitation may stimulate a large loop in phase space before the element goes back to the fixed point. For $0.003 > e_{ij} > -0.083$ the element is in the oscillatory regime $O$ and for $e_{ij} < -0.089$ one finds the excitable regime $\tilde{E}$. Between the excitable regimes and the oscillatory regime small areas in parameter space exist, where a stable focus and a stable limit cycle coexist [white bands in Fig. 4.1(a)]. These additional regimes ($O3$ and $\tilde{O}3$) are not important for the investigations presented in this section. The discussion in this paragraph shows that an oscillatory net of FHN elements with additive variability is a mixture of oscillatory and excitable elements [Fig. 4.1(a)]. The probability $p(\sigma_{v,e})$ for an element to be in one of the three important dynamical regimes depends on $\sigma_{v,e}$ [Fig. 4.1(b)].

Looking at the elements in the heterogeneous nets studied in this section one does not find elements, which rest in their fixed point. All of them show an oscillatory dynamics. Due to the diffusive coupling the excitable elements are forced to spike continuously [see e.g. Fig. 4.5(a)-(f)]. This limit cycle motion in the two dimensional phase space allows to define a phase-angle for each element in the net [41]. The term phase-synchronisation used in this section states that all elements in the net have the same position on the limit cycle and thus the same phase. The term phase wave defines moving patterns in the oscillatory net, where one finds a nontrivial phase difference between the elements. A cut perpendicular to the wave front shows a monoton distribution of the phase angles of the elements. The phase difference $2\pi$ to the starting element defines the wave length $\lambda_p$, which is given in the number of elements. To investigate the pattern formation and the phase synchronisation in a net of FHN elements it is sufficient to study the amplitudes $u_{ij}(t)$ [or $v_{ij}(t)$]. If all elements have the same amplitude for all times then they oscillate in phase. For this consideration it is crucial that the noise and the variability have no strong influence on the form of the limit cycle.

In a first step the influence of the strength of the additive noise $\sigma_{n,e}$ and the strength of the additive variability $\sigma_{v,e}$ on the synchronisation of a net with $N = 128$ and $q = 10$ is studied. The order parameter $R$ [Eq. (2.21)], a measure for the synchronisation,

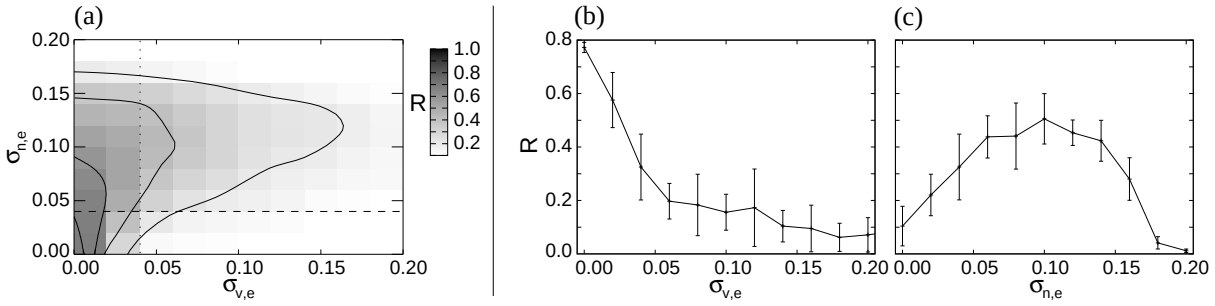


Figure 4.2. The order parameter $R$ [Eq. (2.21)] for a net of FitzHugh-Nagumo elements [Eqs. (3.1)] with diffusive coupling [Eq. (2.18)] averaged over ten realisations of the net for $q = 10$ and $N = 128$. (a): In dependency on the noise strength $\sigma_{n,e}$ and the variability strength $\sigma_{v,e}$, (—) $R = 0.8$, 0.6, 0.4 and 0.2, (- -) $\sigma_{n,e} = 0.04$ and (· ·) $\sigma_{v,e} = 0.04$. (b): In dependency on the variability strength $\sigma_{v,e}$ for $\sigma_{n,e} = 0.04$. (c): In dependency on the noise strength $\sigma_{n,e}$ for $\sigma_{v,e} = 0.04$.

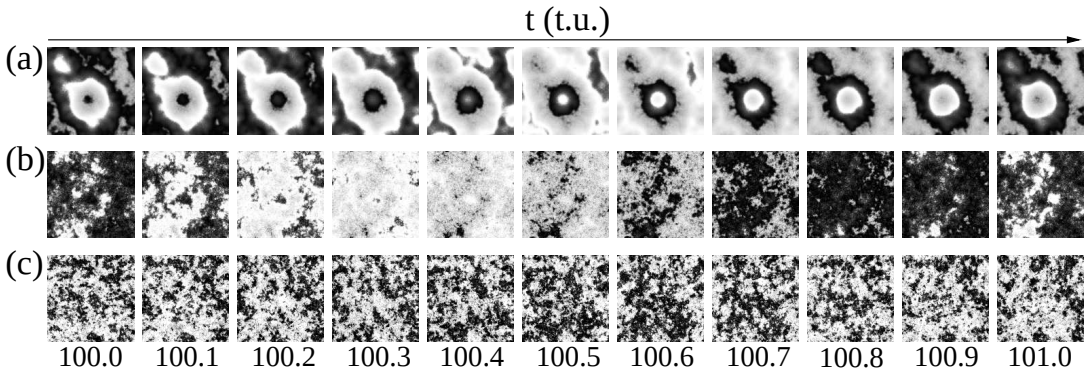


Figure 4.3. Snapshots of $u_{ij}(t)$ for a net of FHN elements [Eqs. (3.1)] with diffusive coupling [Eq. (2.18)] in dependency on the integration time $t$ for random initial conditions, $\sigma_{v,e} = 0.04$, $q = 10$ and $N = 128$. (a): $\sigma_{n,e} = 0$. (b): $\sigma_{n,e} = 0.1$. (c): $\sigma_{n,e} = 0.2$.

is plotted in Fig. 4.2(a) in dependency on these two parameters. Without noise and variability the net can oscillate in a completely synchronised manner [Fig. 2.7(a) for $N = 256$ and $q = 20$] and $R$ is maximal [Fig. 4.2(a)]. If one follows the $\sigma_{v,e}$-axis ($\sigma_{n,e} = 0$) one discerns that $R$ is monotonously decreasing for a growing variability strength and already for a small values $\sigma_{v,e} \approx 0.04$ the synchronisation is almost lost. This loss of the global synchronisation is due to the fact that the variability generates phase waves in the diffusively coupled oscillatory net [Fig. 4.3(a)]. The net with variability is a mixture of excitable and oscillatory elements and due to the local coupling the oscillating elements drag the excitable ones out of their stable focus and force them to spike continuously. This process leads to fixed phase differences between the oscillatory and the spiking excitable elements. This phase differences and the spatial distribution of the elements lead to the emergence of the observed patterns. The variability induced pattern formation can also be observed, if additionally weak additive noise is applied, for example $\sigma_{n,e} = 0.04$ [Figs. 4.2(b) and 4.4(b)]. In this case the coherent phase waves emerge for larger values of the variability strength and the slope of the monotonous decrease of the order parameter $R$ is smaller [Fig. 4.2(a)].

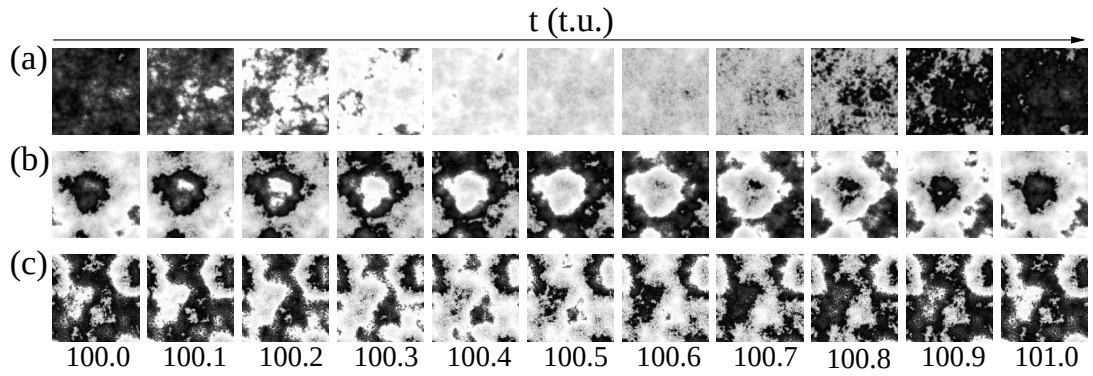


Figure 4.4. Snapshots of $u_{ij}(t)$ for a net of FHN elements [Eqs. (3.1)] with diffusive coupling [Eq. (2.18)] in dependency on the integration time $t$ for random initial conditions, $\sigma_{n,e} = 0.04$, $q = 10$ and $N = 128$. (a): $\sigma_{v,e} = 0$. (b): $\sigma_{v,e} = 0.06$. (c): $\sigma_{v,e} = 0.2$.

The additive noise has a completely different influence on the net dynamics than the additive variability. This is displayed in Fig. 4.4(a). No fixed phase differences between the identical single elements emerge and thus the noise does not induce coherent pattern formation. For growing $\sigma_{n,e}$ the noise more and more disturbs the global oscillation and hence for a net without variability the order parameter $R$ is monotonously decreasing. The slope of this decrease is however much smaller for growing $\sigma_{n,e}$ than for growing $\sigma_{v,e}$.

The interplay of the additive stochastic terms leads to an nontrivial effect. Looking, for instance, at the case $\sigma_{v,e} = 0.04$ [Fig. 4.2(c) and dotted line in Fig. 4.2(a)] one discerns that increasing $\sigma_{n,e}$ starting with $\sigma_{n,e} = 0$ leads now to an increase of $R$ and hence to a more synchronised net dynamics. For an intermediate noise strength the order parameter $R$ has a pronounced maximum at $\sigma_{n,e} \approx 0.1$ and the heterogeneous net oscillates most synchronously. For larger noise strengths the noise-induced synchronisation is gradually destroyed. $R$ is thus decreasing for $\sigma_{n,e} > 0.1$ and tends to zero.

To substantiate this nontrivial effect of the noise several time series for $\sigma_{v,e} = 0.04$ are composed in Fig. 4.5. The first row shows time series of the fast variable for a randomly chosen element of the net for three different noise strengths. The time series depict the dynamics of oscillatory and excitable elements, but it is not possible to identify the dynamical regime of the single elements in the figure, because the excitable ones spike continuously. For $\sigma_{n,e} = 0$ the single element oscillates regularly [Fig. 4.5(a)]. For a growing noise strength the oscillation of the element is more and more disturbed and its time series becomes more irregular [Fig. 4.5(b) and (c)]. The second row shows time series of ten randomly chosen elements of the net. For $\sigma_{n,e} = 0$ the elements oscillate regularly, but not in phase [Fig. 4.5(d)]. The heterogeneous net generates phase waves and there are fixed phase differences between the single elements in the net. At the maximum of $R$, for $\sigma_{n,e} \approx 0.1$, the elements oscillate in phase [Fig. 4.5(e)], in spite of the fact that the single elements do not oscillate as regular as for smaller noise strengths. For $\sigma_{n,e} = 0.2$ the oscillation of each element is strongly influenced by the noise and consequently the noise-induced phase synchronisation is lost [Fig. 4.5(f)]. In the last row of Fig. 4.5 the mean-field of the fast variable is plotted. The large maximal amplitude of $\bar{u}(t)$ for $\sigma_{n,e} = 0.1$ [Fig. 4.5(h)] compared to the cases $\sigma_{n,e} = 0$ [Fig. 4.5(g)] and $\sigma_{n,e} = 0.2$ [Fig. 4.5(i)] confirms the strong phase synchronisation in the net for intermediate noise strengths.

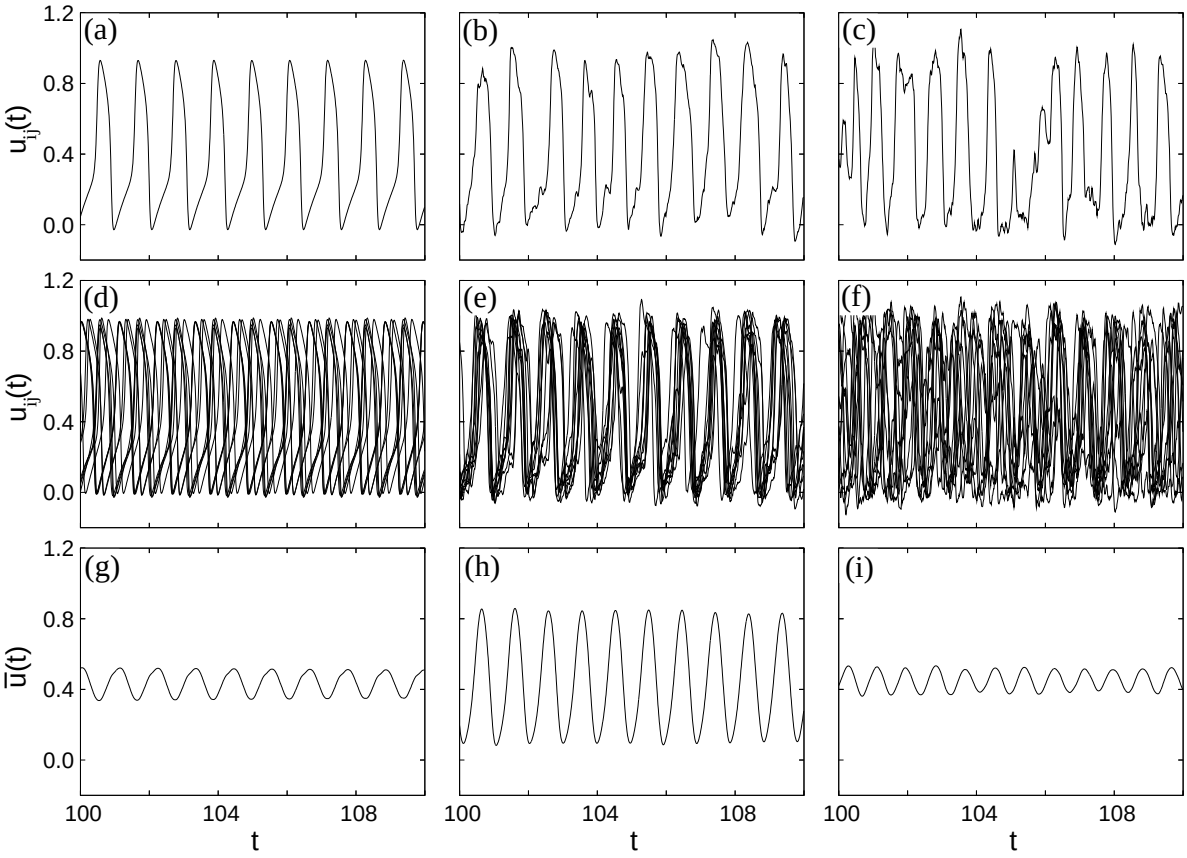


Figure 4.5. Time series for a net of FHN elements [Eqs. (3.1)] with diffusive coupling [Eq. (2.18)] for random initial conditions, $\sigma_{v,e} = 0.04$, $q = 10$ and $N = 128$. (a)-(c): $u_{ij}(t)$ for one randomly chosen element. (d)-(f): $u_{ij}(t)$ for ten randomly chosen elements. (g)-(i): The mean field of the fast variable $\bar{u}(t)$ [Eq. (2.17)]. For each row from left to right: $\sigma_{n,e} = 0$, 0.1 and 0.2.

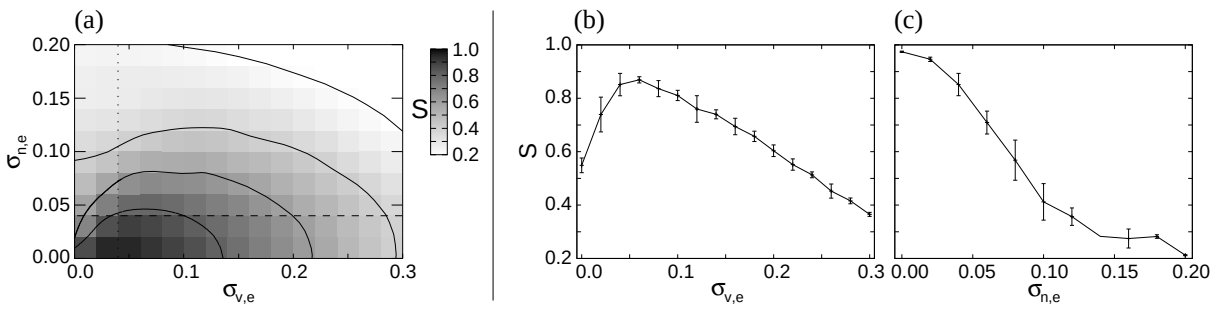


Figure 4.6. The cross correlation $S$ [Eq. (2.24)] for a net of FitzHugh-Nagumo elements [Eqs. (3.1)] with diffusive coupling [Eq. (2.18)] averaged over ten realisations of the net for $q = 10$ and $N = 128$. (a): In dependency on the noise strength $\sigma_{n,e}$ and the variability strength $\sigma_{v,e}$, (—) $S = 0.8$, 0.6, 0.4 and 0.2, (- -) $\sigma_{n,e} = 0.04$ and (· ·) $\sigma_{v,e} = 0.04$. (b): In dependency on the variability strength $\sigma_{v,e}$ for $\sigma_{n,e} = 0.04$. (c): In dependency on the noise strength $\sigma_{n,e}$ for $\sigma_{v,e} = 0.04$.

Without noise the variability can induce pattern formation in the net [Fig. 4.3(a)], because of the fixed phase difference between the oscillatory and the spiking excitable elements. Driving an excitable element with additive noise also leads to the development of spikes, where the spiking is most regular for intermediate noise strengths. This phenomenon is well known as coherence resonance [9]. The excitable elements thus spike continuously for adequate values of $\sigma_{n,e}$ and the fixed phase differences between the elements do not exist anymore. The diffusive coupling leads to the phase synchronisation between the oscillatory and the noise driven excitable elements. In the heterogeneous net a growing noise strength leads thus to a more regular global oscillation and the destruction of the coherent variability-induced patterns. For $\sigma_{n,e} = 0.1$ [Fig. 4.3(b) and Fig. 4.5(h)] the elements are maximally synchronised. This phenomenon has similarities with the noise induced synchronisation in excitable media reported in [41]. For a larger noise strength [$\sigma_{n,e} = 0.2$ in Fig. 4.3(c)] the noise dominates the net dynamics. The single elements do not oscillate regularly anymore and the noise-induced phase synchronisation is lost.

In a next step the pattern formation in a net with $N = 128$ and $q = 10$ is quantified using the cross correlation $S$ [Eq. (2.24)], which is plotted in dependency on the noise strength and the variability strength in Fig. 4.6(a). Following the $\sigma_{n,e}$-axis ($\sigma_{v,e} = 0$) one discerns that $S$ is monotonously decreasing for a growing noise strength indicating that the noise destroys the local order in the net [Fig. 4.4(a)] and no coherent pattern formation is induced. For $\sigma_{v,e} \neq 0$, for example $\sigma_{v,e} = 0.04$ in Fig. 4.6(c), the variability induces pattern formation. These patterns are stable even under the influence of weak noise, as can be seen in Fig. 4.4(b), and the decrease of $S$ is thus small for $\sigma_{n,e} < 0.05$. For larger noise strengths the variability induced patterns are destroyed and the measure $S$ tends to zero.

If one studies a growing variability strength applying additionally a weak additive noise, for example $\sigma_{n,e} = 0.04$ [Fig. 4.6(b) and dashed line in Fig. 4.6(a)], one observes a nontrivial dependency of $S$ on $\sigma_{v,e}$. Increasing the variability strength starting with $\sigma_{v,e} = 0$ leads to an increase of $S$, because the variability induces coherent pattern formation in the net [Fig. 4.4(a)-(c)]. This variability-induced pattern formation is a resonance-like effect. The most coherent phase waves are found for intermediate values of the variability

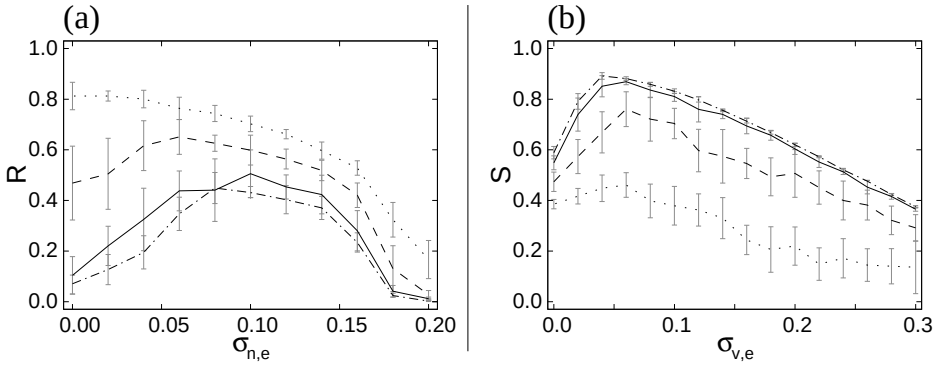


Figure 4.7. $R$ and $S$ for nets of FHN elements [Eqs. (3.1)] with diffusive coupling [Eq. (2.18)] for different side lengths $N$ averaged over ten realisations of the net for $q = 10$. $(\cdot\ \cdot)$ $N = 32$, (- -) $N = 64$, (—) $N = 128$ and (- $\cdot$ -) $N = 256$. (a): The order parameter $R$ in dependency on $\sigma_{n,e}$ for $\sigma_{v,e} = 0.04$. (b): The cross correlation $S$ in dependency on $\sigma_{v,e}$ for $\sigma_{n,e} = 0.04$.

strength and one discerns a maximum of the cross correlation for $\sigma_{v,e} \approx 0.06$. For even larger values of $\sigma_{v,e}$ the variability still induces pattern formation, but the coherence of the phase waves is more and more lost [Fig. 4.4(c)] and the measure $S$ is decreasing.

The variability-induced patterns have a determined length-scale, the wave length $\lambda_P$, and the side length of the net $N$ has to be at least of the size of $\lambda_P$ to observe coherent pattern formation. For the coupling strength $q = 10$ one finds $\lambda_P \approx 60$ [see Fig. 4.3(a)]. If one studies for instance nets with $N = 32$ (Fig. 4.7) the variability cannot generate phase waves and thus the noise-induced synchronisation cannot be observed in the heterogeneous net [Fig. 4.7(a)]. In this case a growing noise strength for $\sigma_{v,e} = 0.04$ leads to a monotonous decrease of $R$. Furthermore one does not find a peak of the cross correlation for a growing variability strength and $\sigma_{n,e} = 0.04$ [Fig. 4.7(b)]. For a growing net size the measure $S$ is increasing for all values of the variability strength and for intermediate values of $\sigma_{v,e}$ a peak of the cross correlation emerges. Comparing the results for the side lengths $N = 128$ and $N = 256$ one finds that the quantities $R$ and $S$ do hardly change. This indicates that the pattern formation and thus the noise-induced synchronisation is not strongly effected by the side length $N$, if the net is large enough to support the variability induced patterns.

The results presented in this section hold for a wide range of the coupling strength, as can be seen in Fig. 4.8. Increasing the noise strength for $\sigma_{v,c} = 0.04$ the peak in $R$ is shifted to larger values of $\sigma_{n,e}$ for larger values of the coupling strength [Fig. 4.8(a)]. Furthermore one needs larger values of the variability strength to induce the coherent pattern formation and thus to destroy the synchronisation. For that reason one finds a larger value of $R$ in Fig. 4.8(a) for $\sigma_{n,e} = 0$ and $q = 20$ compared to the smaller coupling strengths. For $q = 20$ one finds a more pronounced maximum of $R$ in dependency on $\sigma_{n,e}$ for a larger value of the variability strength (not shown here). The cross correlation in dependency on the variability strength remains almost unchanged, if the coupling strength is increased [Fig. 4.8(b)]. The coherence of the variability induced patterns is thus nearly independent of the coupling strength. The wave length of the variability-induced phase waves slightly increases for larger values of $q$ and one needs therefore slightly larger nets to observe pattern formation.

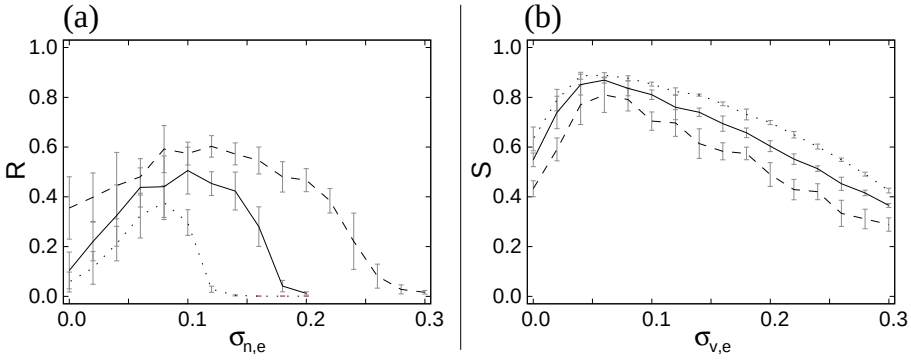


Figure 4.8. $R$ and $S$ for nets of FHN elements [Eqs. (3.1)] with diffusive coupling [Eq. (2.18)] for different coupling strengths $q$ averaged over ten realisations of the net for $N = 128$. $(\cdot\ \cdot)$ $q = 5$, (—) $q = 10$ and (- -) $q = 20$. (a): The order parameter $R$ in dependency on $\sigma_{n,e}$ for $\sigma_{v,e} = 0.04$. (b): The cross correlation $S$ in dependency on $\sigma_{v,e}$ for $\sigma_{n,e} = 0.04$.

The ability of additive variability to induce coherent patterns in oscillatory nets with diffusive coupling is quite general. Pattern formation was for example studied in a chain of chemical oscillators [22] and one finds results similar to the ones presented in the Figs. 4.6, 4.3(a) and 4.4 also for a diffusively coupled net of phase-oscillators. In the latter case the variability has a big influence on the frequency of the single oscillators. The local interplay of these elements with different frequencies leads to the emergence of coherent patterns. However additive noise does not destroy the patterns in heterogeneous nets of phase-oscillators, thus a more synchronised net dynamics does not occur.

## 4.2 Multiplicative Variability and Multiplicative Noise

In difference to Section 4.1 multiplicative noise and white multiplicative variability [Eqs. (3.3)] are studied in this section neglecting the additive stochastic influences ($\sigma_{n,e} = 0$ and $\sigma_{v,e} = 0$). The investigations are done varying the side length of the net $N$, the coupling strength $q$, the noise strength $\sigma_{n,c}$ and the variability strength $\sigma_{v,c}$.

A net of FitzHugh-Nagumo elements with variability in parameter $c$ is again a mixture of elements in different dynamical regimes [Fig. 2.5(a) and Fig. 4.9(a)]. For $4.53 \leq c_{ij} \leq 5.15$ the single element is in the oscillatory regime $O$, for $c_{ij} > 5.19$ in the excitable regime $\tilde{E}$ and for $0 \leq c_{ij} < 4.41$ in the excitable regime $E$. For $c_{ij} < 0$ the dynamics of the element completely changes, causing the system and thus the numerical integration to get unstable. Consequently the parameter values $c_{ij} < 0$ have to be excluded by setting the probability distribution $P(c, \sigma_{v,c})$ to zero for corresponding values of $c$. To preserve the symmetry of the probability distribution values of the parameter $c$ greater then $2C$ are excluded as well [cut-off in Fig. 4.9(a)]. For $\sigma_{v,c} = 2.2$, the largest variability strength used in this section, this means that approximately 4% of the Gaussian distributed $c_{ij}$ are discarded. The probability to be in one of the three main regimes, which is plotted in Fig. 4.9(b), depends on the variability strength $\sigma_{v,c}$. Between the excitable regimes and the oscillatory regime one again finds small regions in parameter space with the additional dynamical regimes $O3$ and $\tilde{O}4$ [white bands in Fig. 4.9(a)]. The regime $O3$, where a stable focus and a stable limit cycle coexist, is of some importance for the transition from oscillatory to excitable net dynamics.

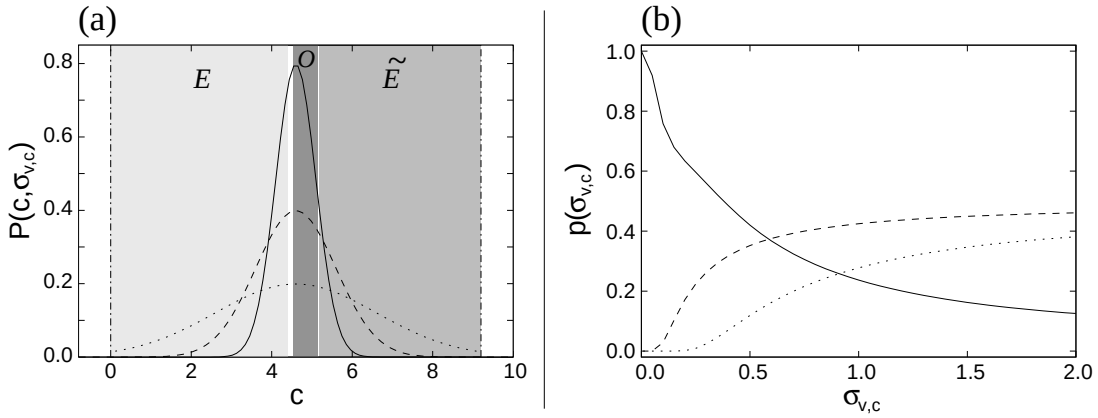


Figure 4.9. (a): The Gaussian probability distribution $P(c, \sigma_{v,c})$, for three different values of the variability strength, (—) $\sigma_{v,c} = 0.5$, (- -) $\sigma_{v,c} = 1$ and $(\cdot\ \cdot)$ $\sigma_{v,c} = 2$. $(\cdot$ - $\cdot)$ cut-off of the probability distribution. The grey areas mark the dynamical regimes. (b): Probability $p(\sigma_{v,c})$ for one FitzHugh-Nagumo element to be in the oscillatory regime $O$ (—), the excitable regime $E$ (- -) and the excitable regime $\tilde{E}$ $(\cdot\ \cdot)$, in dependency on the variability strength $\sigma_{v,c}$.

Comparing Fig. 4.9 with Fig. 4.1 one sees that the composition of the net for the given parameters, concerning the proportion of elements in the different dynamical regimes, is quiet similar for additive and for multiplicative variability. Nevertheless the multiplicative variability has a much different influence on the net dynamics. The reason for this difference is a systematic influence of the multiplicative stochastic terms on the net dynamics. This systematic influence can be approximated using Eq. (3.10). This equation provides a value for the effective parameter $\langle c \rangle$, which may determine the dynamics of the net. The result of Eq. (3.10) is plotted in Fig. 4.10 in dependency on $\sigma_{n,c}$ and $\sigma_{v,c}$.

The influence of the multiplicative noise on the effective parameter $\langle c \rangle$ is displayed in Fig. 4.10(a). One clearly discerns a monoton decrease of this parameter for a growing noise strength. Comparing this result with the linear stability analysis [Fig. 2.5(a)] one can predict a transition from oscillatory dynamics to excitable dynamics. One expects to find the oscillatory regime $O$ for $\sigma_{n,c} < 0.09$ and the excitable regime $E$ for $\sigma_{n,c} > 0.13$. Between these two regimes the regime $O3$, in which the net can either oscillate or rest in its fixed point, exists. A diffusively coupled net in the excitable regime $E$ can show either excitable dynamics or subexcitable dynamics. Studying a homogeneous net changing the value of parameter $c$ one can find a critical value in dependency on the coupling strength $q$, for which this transition occurs. Comparing this value with $\langle c \rangle$ one expects a transition to subexcitable net dynamics for $\sigma_{n,c} \approx 0.28$ if $q = 50$ [(- -) in Fig. 4.10(a)].

The multiplicative variability has a similar influence on the effective parameter as the multiplicative noise [Fig. 4.10(b)], the value of $\langle c \rangle$ is monotonously decreasing for growing $\sigma_{v,c}$. According to this systematic effect the dynamics of the net is predicted to be oscillatory for $\sigma_{v,c} < 0.57$ and excitable for $\sigma_{v,c} > 0.92$. Between these regimes one again has the regime $O3$, for which one expects the coexistens of a limit cycle and a stable fixed point. The transition from the excitable to the subexcitable net dynamics is expected for $\sigma_{v,c} \approx 1.8$ if $q = 50$ [(- -) in Fig. 4.10(b)]. The combined systematic influence of the multiplicative noise and the multiplicative variability on the parameter $\langle c \rangle$ is depicted in Fig. 4.10(c). One again sees that according to the prediction from Eq. (3.10) the net passes

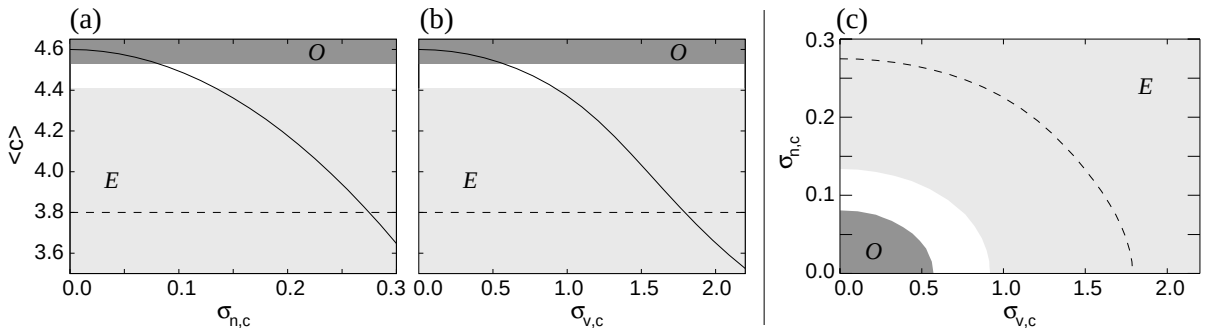


Figure 4.10. Effective mean value $\langle c \rangle$ (—) [Eq. (3.10)] and corresponding dynamical regimes for nets of FHN elements [Eqs. (3.1)], (- -) expected transition from $E_H$ to $E_S$ for $q = 50$. The grey areas mark the dynamical regimes. (a): In dependency on the noise strength $\sigma_{n,c}$ for $\sigma_{v,c} = 0$. (b): In dependency on the variability strength $\sigma_{v,c}$ for $\sigma_{n,c} = 0$. (c): In dependency on the noise strength $\sigma_{n,c}$ and the variability strength $\sigma_{v,c}$.

through transitions from oscillatory dynamics to excitable and subexcitable behaviour, if the strengths of the multiplicative stochastic terms is increased. The borders of the dynamical regimes show an elliptical symmetry in dependency on the strength of the multiplicative noise and the multiplicative variability.

To verify the predictions from Eq. (3.10) simulations of oscillatory nets of globally coupled FHN elements for different side lengths $N$ and different coupling strengths $q$ are performed. For the random initial conditions used for these numerical calculations a net of FHN elements in the regime $O3$ is hardly ever resting in its fixed point. The stable fixed point is only found in the regime $E$, where the limit cycle has vanished. To identify the transition from oscillatory dynamics to excitability the relative resting time $T_r$ [Eq. (2.20)] and the time averaged mean field $M$ [Eq. (2.19)] of the variable $u(t)$ are used as oder parameters. The transition is associated with a jump of the mean field from $M > 0.40$ to $M < 0.24$. In the following this jump is marked by a contour-line for $M = 0.25$, which is denoted as $M_c$. To display that a net in the regime $E$ is excitable and not subexcitable one additionally has to show that the elements of the net are in the part of phase space, where an excitation is possible [10]. For that reason the relative resting time $T_r$ of all elements of the net in this special part of phase space is used. The transition from oscillatory dynamics to the regime $E$ corresponds with a jump of the resting time from $T_r < 0.5$ to $T_r > 0.98$ and is marked by a contour-line for the value $T_r = 0.98$, where this contour-line is denoted as $T_{r,c}$. Once in the exitable regime a further increase of the strengths of the multiplicative stochastic terms leads to a slow monoton decrease of $T_r$ and one again intersects the contour line $T_{r,c}$. The second intersection marks the transition from an excitable net to a subexcitable net. One has to notice here that the transition to the subexcitable regime does not cause a jump of the relative resting time and can hence only be shown qualitatively [11, 38].

The contour-lines $M_c$ and $T_{r,c}$ are displayed in Fig. 4.11 for nets with multiplicative noise, but without variability. The predicted dynamical regimes, according to Eq. (3.10), are given by the grey areas in the figure. For small values of the noise strength one finds $M > 0.25$, the elements in the net show oscillatory dynamics. Increasing the noise strength, e.g. for a net with $N = 50$ and $q = 50$, one finds a sudden jump in the value of the mean field (marked by $M_c$), where the transition from oscillatory to excitable net

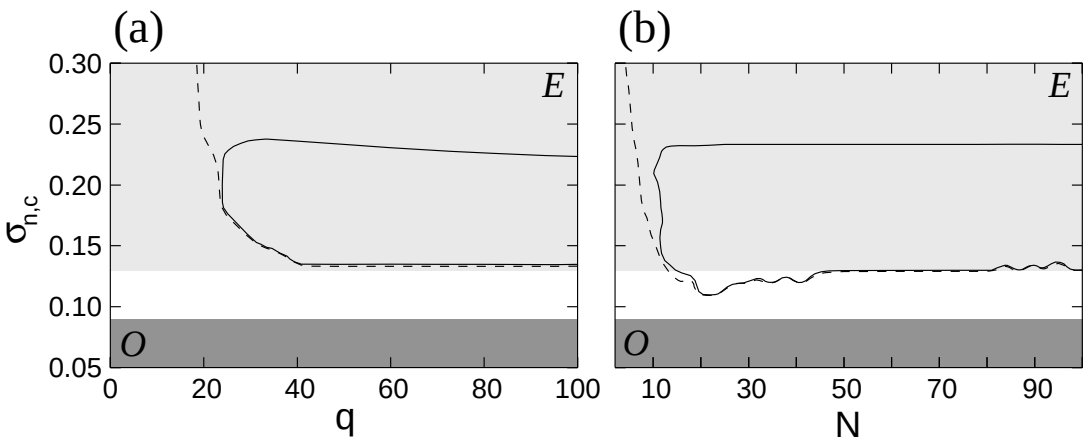


Figure 4.11. The relative resting time [Eq. (2.20)] and the time averaged mean field [Eq. (2.19)] for a net of FHN elements [Eqs. (3.1)] with global coupling [Eq. (2.16)] in dependency on the noise strength $\sigma_{n,c}$ for $\sigma_{v,c} = 0$, (—) $T_r = 0.98$ ($T_{r,c}$), (- -) $M = 0.25$ ($M_c$). The grey areas are the predictions from Eq. (3.10). (a): In dependency on the coupling strength $q$ for $N = 50$. (b): In dependency on the side length $N$ for $q = 50$.

dynamics occurs. For $M < M_c$ all elements rest in the focus, which is unstable without the multiplicative noise. The transition, and thus the contour-line $M_c$, strongly depends on the coupling strength [Fig. 4.11(a)] and the side length of the net [Fig. 4.11(b)]. For a large coupling strength and a sufficiently large net size one finds the transition at the predicted value of $\sigma_{n,c}$. Decreasing the coupling strength the transition occurs for larger values of $\sigma_{n,c}$ and for $q < 20$ the transition cannot be found. A strong coupling is necessary to minimise the random influences of the noise and to stabilise the net in the fixed point. Changing the net size for $q = 50$ one finds a similar behaviour of $M_c$. It is clearly visible, that a minimal side length $N \approx 10$ is necessary to find the noise induced excitability (NIE). The dynamics of a small net is not determined by the systematic effect, but by the remaining random influences of the noise and hence NIE cannot be observed [10, 11]. A large ensemble of coupled elements is thus necessary to observe NIE. The larger the net the better the random influences of the noise are averaged out. For a sufficiently large $N$ the transition occurs at the predicted value of $\sigma_{n,c}$.

The relative resting time additionally indicates a transition from the excitable to the subexcitable net dynamics for large noise strengths. This transition is found in the simulations of large nets with sufficiently strong coupling for $\sigma_{n,c} \approx 0.23$. This corresponds qualitatively with the predictions presented in Fig. 4.10.

For nets without noise but in presence of the variability (Fig. 4.12) the elements of the net are in different dynamical regimes and hence they exhibit diverse dynamics without coupling. Nevertheless for sufficiently large coupling strengths nets with $N \geq 20$ show a spatially uniform temporally oscillatory net dynamics for $\sigma_{v,c} < 0.9$. Increasing the variability strength for such a net a transition from oscillatory to excitable net dynamics is found. For a strong coupling ($q \geq 50$) the transition to the variability induced excitability (VIE) occurs near the value of $\sigma_{v,c}$ predicted by Eq. (3.10), however the convergence towards the predicted value is slower than for multiplicative noise [Fig. 4.12(a)]. This convergence nevertheless confirms the presumption, that the dynamics of the large heterogeneous net with strong coupling is determined by the parameter $\langle c \rangle$, which is systematically changed by the variability strength [Fig. 4.10].

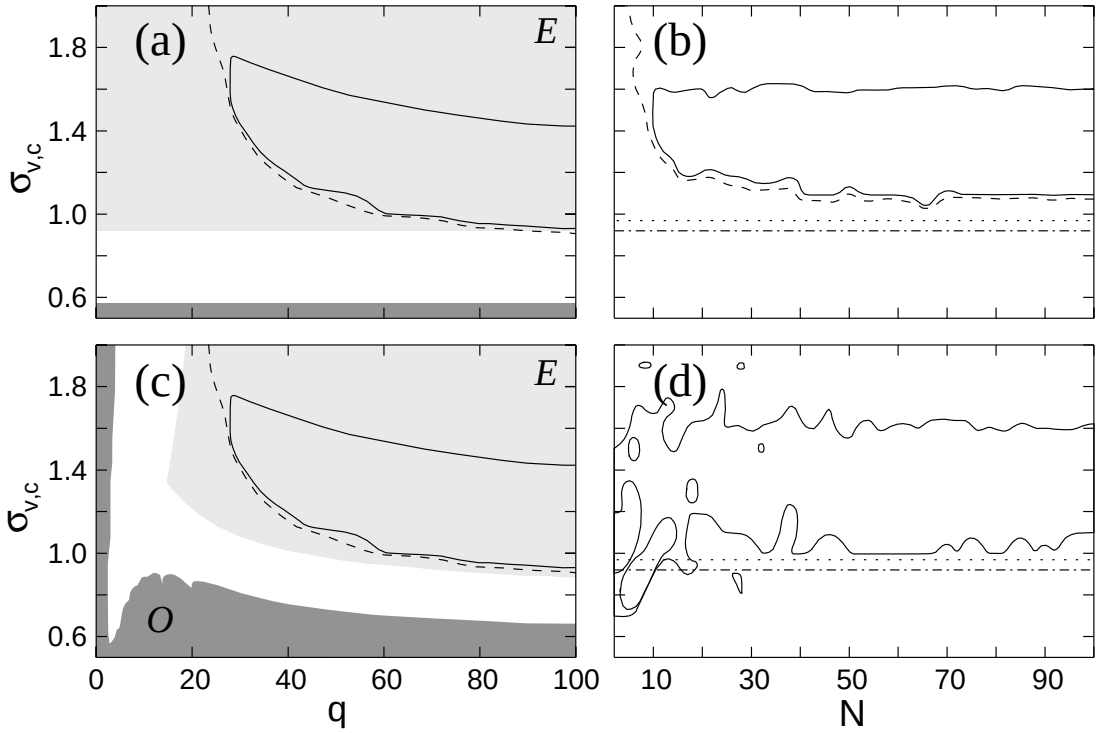


Figure 4.12. The relative resting time [Eq. (2.20)] and the time averaged mean field [Eq. (2.19)] for a net of FHN elements [Eqs. (3.1)] with global coupling [Eq. (2.16)] in dependency on the variability strength $\sigma_{v,c}$ for $\sigma_{n,c} = 0$, (—) $T_{r,c}$, (- -) $M_c$. (a), (c): In dependency on the coupling strength $q$ for $N = 50$, averaged over ten realisations of the net. The grey areas are the predictions from Eq. (3.10) in (a) and from Eqs. (3.11) in (c). (b), (d): In dependency on the side length $N$ for $q = 50$. Averaged over ten realisations of the net in (b) and for one realisation in (d). Predicted transition to excitable dynamics ($\cdot$ - $\cdot$) from Eq. (3.10) and ($\cdot$ $\cdot$) from Eqs. (3.11).

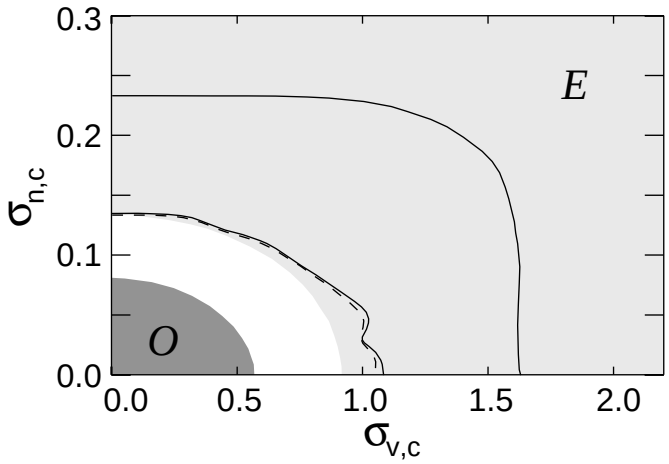


Figure 4.13. The relative resting time [Eq. (2.20)] and the time averaged mean field [Eq. (2.19)] for a net of FHN elements [Eqs. (3.1)] with global coupling [Eq. (2.16)] in dependency on $\sigma_{n,c}$ and $\sigma_{v,c}$ with $N = 50$ and $q = 50$, averaged over ten realisations of the net, (—) $T_{r,c}$, (- -) $M_c$. The grey areas are the predictions from Eq. (3.10).

For smaller values of the coupling strength the mean field approximation [Eqs. (3.11)] allows a more precise prediction of the transition to excitable net dynamics than Eq. (3.10). The results of a stability analysis of the mean field approximation in dependency on the variability strength and the coupling strength is plotted in Fig. 4.12(c). This stability analysis reveals that the excitable regime can only be found for coupling strengths greater than $q \approx 20$. Furthermore one sees the expected decrease of the border between the regimes $E$ and $O3$ for a growing coupling strength and $q > 20$. This is in qualitative agreement with the numerical results for $M_c$ and $T_{r,c}$ [Fig. 4.12(c)].

The boundaries of the VIE regime do also depend on the side length of the net [Fig. 4.12(b) and (d)]. For small $N$ no clear contour lines $M_c$ and $T_{r,c}$ exist for a single net and the border of the transition to excitability is not well defined [Fig. 4.12(d)]. The reason for this phenomenon is that for small nets the parameter $\langle c \rangle$ for a given net can strongly differ from the prediction and thus the dynamical regime is not completely determined by the variability strength $\sigma_{v,c}$. Increasing the side length $N$ the effective parameter of the net converges towards the prediction and hence for a sufficiently large $N$ one finds a clear transition from an oscillatory to an excitable net. In Fig. 4.12(d) such a clear transition is visible for nets with $N \gtrsim 40$. This result reveals that the predictions from Eq. (3.10) and Eqs. (3.11) are only valid for large nets. One possibility to get a better statistics even for small values of $N$ and thus well defined contour lines $M_c$ and $T_{r,c}$ is to average over several realisations of the net. This is done in Fig. 4.12(b) for ten realisations and one discerns that the mean field approximation yields a slightly better prediction of the resulting contour lines than the parameter $\langle c \rangle$.

In a next step the combined influence of the multiplicative noise and the multiplicative variability on a large net ($N = 50$) with a strong coupling ($q = 50$) is studied. The results are plotted in Fig. 4.13. The contour line $M_c$, now a function of $\sigma_{n,c}$ and $\sigma_{v,c}$, reveals a elliptical symmetry as predicted by Eq. (3.10). Furthermore the numerical results correspond very good with the theoretical prediction of the transition to oscillatory dynamics. In Fig. 4.13 the contour line $T_{r,c}$ divides the parameter space in three distinct areas. For small $\sigma_{n,c}$ and/or $\sigma_{v,c}$ the net is oscillatory. For parameter values, which

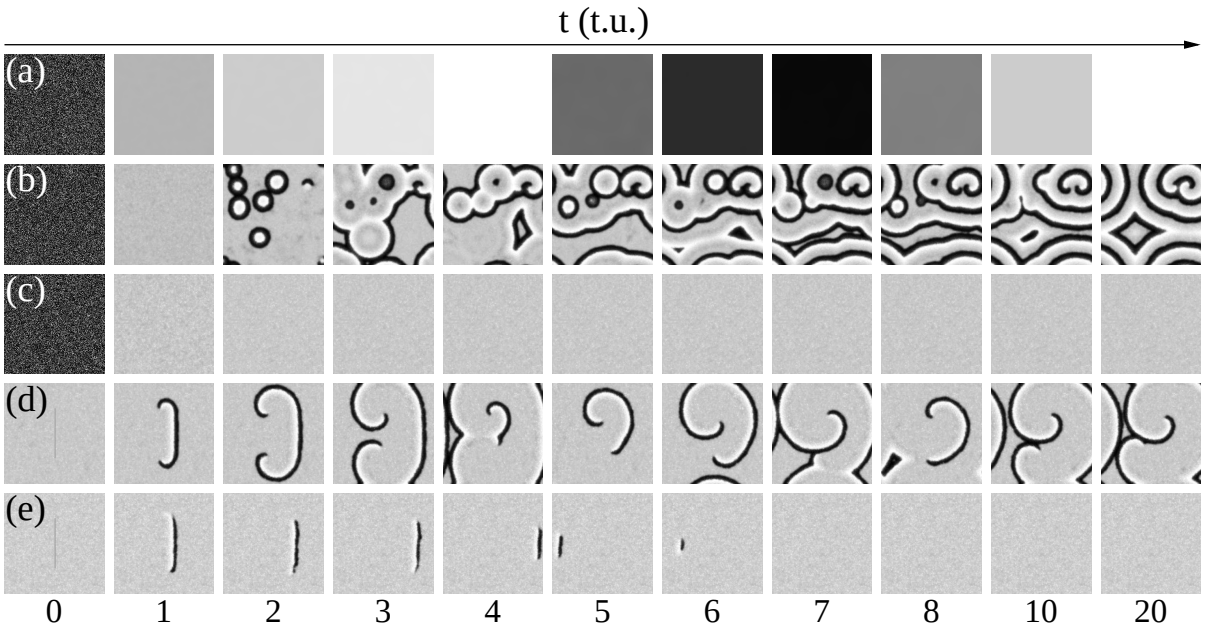


Figure 4.14. Snapshots of $u_{ij}(t)$ for a net of FHN elements [Eqs. (3.1)] with diffusive coupling [Eq. (2.18)] in dependency on the integration time $t$ and the variability strength $\sigma_{v,c}$ for $N = 256$, $q = 50$ and $\sigma_{n,c} = 0$. (a)-(c): Random initial conditions, (a) $\sigma_{v,c} = 0$, (b) $\sigma_{v,c} = 1.1$ (regime $E_P$) and (c) $\sigma_{v,c} = 1.54$. (d), (e): Initial conditions induce a spiral wave, (d) $\sigma_{v,c} = 1.54$ and (e) $\sigma_{v,c} = 2.2$.

correspond to the area enclosed by $T_{r,c}$, the observed net shows excitable dynamics and for large $\sigma_{n,c}$ and/or $\sigma_{v,c}$ one expects to find the subexcitable regime $E_S$, which is well known for diffusively coupled nets. The border between the excitable and the subexcitable regime corresponds qualitatively with the prediction visible in Fig. 4.10(c).

The results for the globally coupled nets demonstrate that increasing the strengths of the multiplicative stochastic terms in large nets with a strong coupling lead to a clear transition from oscillatory to excitable net dynamics. Knowing the effective parameter $\langle c \rangle$ one can predict this transition, which supports the assumption that a systematic effect of the variability is the reason for the observed transition. All the numerical simulations presented in this section for globally coupled nets are started with random initial conditions, for which a net in the noise and/or variability induced regime $O3$ is hardly ever resting in its fixed point. One nevertheless can find the predicted stable fixed point of the regime $O3$, if one initialises all elements of the net with the values of this fixed point. In this case a large net with a sufficiently strong coupling strength will rest in the noise and/or variability induced stable fixed point of the regime $O3$ for all times and the transition from $O$ to $O3$ is found at the predicted values of the noise and/or the variability strength.

In the following a large oscillatory net ($N = 256$) with diffusive coupling [Eq. (2.18)] is studied to investigate the influence of the multiplicative variability and the multiplicative noise on pattern formation and signal transmission. Based on the results for globally coupled nets the large coupling strength $q = 50$ is chosen for the numerical simulations.

At first the pattern formation is studied in a net without multiplicative noise. Snapshots of such a net for different values of the variability strengths are composed in Fig. 4.14. For values of the variability strength $\sigma_{v,c} < 1$ the simulations reveal a more or less synchronous

oscillatory dynamics for nearly all initial conditions [Fig. 4.14(a)]. For $\sigma_{v,c} \approx 1.0$, the predicted value for the transition to excitability [Fig. 4.10(b)], the net dynamics changes completely and excitation waves appear. These variability induced patterns, which are spiral and circular waves, are typical for excitable nets (Chapter 2). The excitable regime, where the spatially uniform temporally constant solution is not stable, because the diverse net itself or the noise generates patterns (spontaneous pattern formation), which spread through the whole net, is called $E_P$. For $\sigma_{v,c} = 1.1$ the net is in this pattern forming regime [Fig. 4.14(b)]. For larger values of $\sigma_{v,c}$ [Fig. 4.14(c)] the spatially uniform temporally constant solution is found for almost all initial conditions and realisations of the net. Nevertheless excitation waves can still be induced [Fig. 4.14(d)] and hence the net is in the excitable regime $E_H$. The border to the subexcitable net (regime $E_S$), where all excitations die out for $t \to \infty$ [Fig. 4.14(e)], is found for values larger than $\sigma_{v,c} \approx 2$. This value is in qualitative agreement with the prediction presented in Fig. 4.10(b).

Similar pattern forming regimes are found for diffusively coupled oscillatory nets with multiplicative noise and $\sigma_{v,c} = 0$ ($\sigma_{n,c}$-axes in Fig. 4.15). Increasing the noise strength starting from $\sigma_{n,c} = 0$ on finds first oscillatory dynamics, then the excitable regimes $E_P$ and $E_H$ and finally subexcitable net dynamics [11, 38]. The prediction of the transitions using Eq. (3.10), which is plotted in Fig. 4.10(a), is in good agreement with the numerical results [see also $\sigma_{n,c}$-axes in Fig. 4.16(b)).

In a next step the interplay of the multiplicative noise and the multiplicative variability in the diffusively coupled net is studied, where the results are plotted in Fig. 4.15. The borders between the different pattern-forming regimes, which depend now on $\sigma_{n,c}$ and $\sigma_{v,c}$, reveal the expected elliptical symmetry. For small variability and/or noise strengths the net is oscillatory and exhibits nearly synchronous oscillations. In an intermediate range of the variability and/or the noise strength the net dynamics changes completely and one finds pattern formation. The net is now in the excitable regime $E_P$. The excitation waves in the regime $E_P$ are generated by the diverse net or by the multiplicative noise. In nets with weak multiplicative noise ($\sigma_{n,c} < 0.05$) one finds both spiral waves and circular waves. The periodic circular waves are emitted by small oscillating clusters in the diverse net. In nets, where the pattern formation is dominated by the multiplicative noise no periodic circular waves appear, because there are no fixed oscillating clusters in the nets. In such nets stable spiral waves appear and dominate the net dynamics. For slightly larger values of the variability and/or noise strengths the regime $E_H$ is found. This regime can be identified inducing spiral waves with special initial conditions [Fig. 4.14(d)]. For large values of $\sigma_{v,c}$ and/or $\sigma_{n,c}$ all wave fronts die out for large integration times. The net is now in the subexcitable regime $E_S$.

The different dynamical regimes of the net dynamics are presented in detail in Fig. 4.16(a). The elliptical symmetry of the borders between the dynamical regimes, which is predicted by Eq. 3.10 [Fig. 4.10(c)], is clearly visible. In Fig. 4.16(b) the numerical results are directly compared with the predictions based on the effective parameter $\langle c \rangle$. The values of the variability strength and the noise strength, for which the transition from oscillatory to excitable dynamics occurs, can be predicted quiet well, but in the simulations the pattern formation sets in for slightly smaller values of $\sigma_{v,c}$ and/or $\sigma_{n,c}$ than expected. This is especially visible for nets, where the transition is mainly induced by the multiplicative variability. In this case the diverse net, which is predicted to be in the regime $O3$, allows already for pattern formation. The comparison of the numerical result and the prediction of the transition from the excitable regime $E_H$ to the subexcitable regime $E_S$ is also shown in Fig. 4.16(b). This transition can be predicted with a maximal

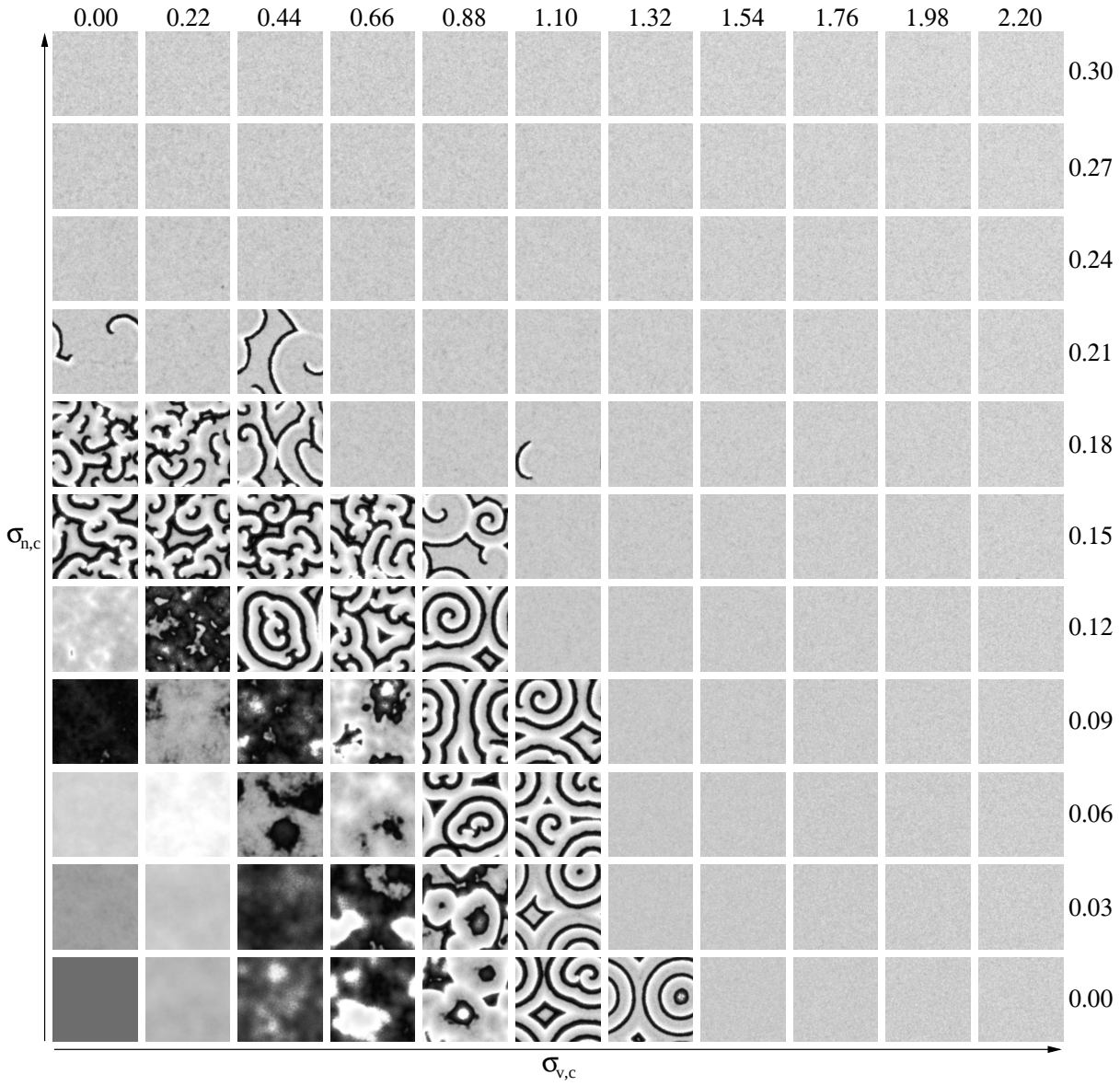


Figure 4.15. Snapshots of $u_{ij}(t)$ for a net of FHN elements [Eqs. (3.1)] with diffusive coupling [Eq. (2.18)] in dependency on the noise strength $\sigma_{n,c}$ and the variability strength $\sigma_{v,c}$ for random initial conditions, the integration time $t = 50t.u.$, $N = 256$ and $q = 50$.

error of about 10%, where the transition is found for larger values of $\sigma_{v,e}$ and/or $\sigma_{n,e}$ in the simulations. Such an error is not surprising, because the transition from $E_H$ to $E_S$ is not as well defined as a transition, which is connected with a change of the dynamical regime of the elements (for instance $O3$ to $E$). To identify the border of the regime $E_S$ one has to induce a spiral wave and a change in the form of the induced wave front can shift the transition to $E_S$ a few percent.

The simulations of diffusively coupled nets of FHN elements substantiate the assumption that $\langle c \rangle$ governs the net dynamics for large nets with strong coupling. One just has to know the value of this effective parameter to predict the dynamical regime of the net.

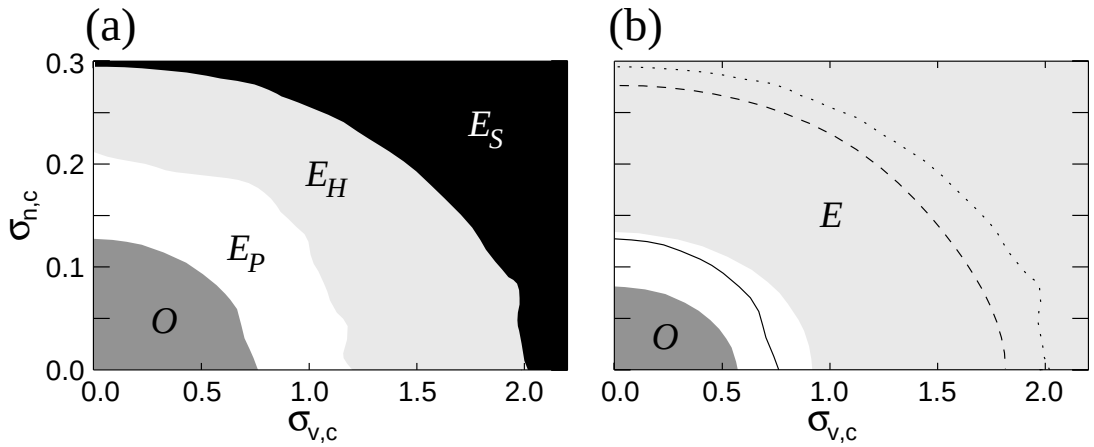


Figure 4.16. The pattern forming regimes of a net of FHN elements [Eqs. (3.1)] with diffusive coupling [Eq. (2.18)] in dependency on the noise strength $\sigma_{n,c}$ and the variability strength $\sigma_{v,c}$ for $N = 256$ and $q = 50$. (a): The simulation results. (b): The comparison of the simulation results with the predictions from Eq. 3.10 (grey areas), (—) numerical result for the transition from $O$ to $E_P$, (- -) expected transition from $E_H$ to $E_S$ [Fig. 4.10(c)], $(\cdot\ \cdot)$ numerical result for the transition from $E_H$ to $E_S$.

## 4.3 Summary and Conclusions

In Section 4.1 it is shown that the interplay of additive variability and additive noise in oscillatory nets strongly influences the net dynamics. The additive variability induces pattern formation and hence even small values of the variability strength destroy the synchronised oscillation the net exhibits without variability. In the heterogeneous oscillatory net the synchronisation can be restored by additive noise, where this noise-induced phase synchronisation exhibits a resonance-like dependency on the noise strength. The variability-induced pattern formation is also a resonance-like effect provided additive noise is present. In this case one finds maximally coherent patterns for intermediate values of the variability strength. To observe the variability-induced patterns the net has to exceed a certain size and thus the net size is important for the noise-induced synchronisation phenomenon.

In contrast to the additive stochastic terms multiplicative variability can induce a transition to excitable and subexcitable dynamics in a large oscillatory net of neural elements with a strong coupling (Section 4.2). This transition, which has a strong influence on the observed pattern formation, is explained by a systematic change of the macroscopic net parameter $\langle c \rangle$. A theoretical expression for this parameter, in dependency on the variability strength, provides a prediction of the border to VIE in the limit of large $N$ and strong coupling. This demonstrates that the variability induced transition of the whole net to the excitable regime is a collective effect, which is not determined by a certain amount of excitable elements in an oscillatory net. A net with additive variability with a similar amount of elements in the excitable regime shows a completely different dynamics and no transition to the regimes $E_P$, $E_H$ and $E_S$ can be found (Section 4.1). In a net with additional multiplicative noise the parameter $\langle c \rangle$ depends on the noise strength as well and so do the borders of the described transitions. In this case the multiplicative noise has a counterintuitive influence on the net dynamics. Increasing the strength of the

noise does lead to a suppression of the net dynamics. For large noise strengths the net rests in the noise induced stable fixed point for all times and no excitations are possible anymore.

In Section 4.2 the variability and the noise act in a similar way. Both lead to the same transition and the observed patterns are alike. This is completely different for the additive variability and the additive noise in Section 4.1. In this section one finds that the influence of the variability and the noise is completely different and their interplay leads to new and unexpected phenomena.

These results demonstrate that the interplay of variability and noise may play an important role in spatially extended oscillatory biophysical systems. Variability and noise may be essential for pattern-forming mechanisms, phase transitions, stochastic resonance effects and synchronisation, where the system size and the coupling strength can be of great importance.